

# Autofib Redshift Survey: II – The Evolution of the Galaxy Luminosity Function by Spectral Type

Jeremy Heyl<sup>1,2\*</sup>, Matthew Colless<sup>3</sup>, Richard S. Ellis<sup>1</sup> and Tom Broadhurst<sup>4,5</sup>

<sup>1</sup>*Institute of Astronomy, Madingley Road, Cambridge CB3 0HA, UK*

<sup>2</sup>*Lick Observatory, Board of Studies in Astronomy and Astrophysics, University of California, Santa Cruz, CA 95064, USA*

<sup>3</sup>*Mount Stromlo and Siding Spring Observatories, The Australian National University, Weston Creek, ACT 2611, Australia*

<sup>4</sup>*Department of Physics and Astronomy, Johns Hopkins University, Baltimore MD 21218, USA*

<sup>5</sup>*Department of Astronomy, University of California, Berkeley, CA 94720, USA*

Accepted —. Received —; in original form —.

## ABSTRACT

We determine the evolution of the galaxy luminosity function (LF) as a function of spectral type using the Autofib redshift survey, a compendium of over 1700 galaxy redshifts in various magnitude-limited samples spanning  $b_J=11.5\text{--}24.0$ . To carry out this analysis we have developed a cross-correlation technique which classifies faint galaxy spectra into one of six types based on local galaxy templates. Tests and simulations show that this technique yields classifications correct to within one type for more than 90% of the galaxies in our sample. We have also developed extensions of the step-wise maximum likelihood method and the STY parametric method for estimating LFs which are applicable to recovering an evolving LF from multiple samples. We compare these methods to the standard  $1/V_{\text{max}}$  method used in Paper I.

Applying these spectral classifications and LF estimators to the Autofib sample, we find that: (i) The spectra and LF of E/S0 galaxies show no appreciable evolution out to at least  $z\sim 0.5$ . (ii) Early-type spirals show modest evolution, characterised by a gradual steepening of the faint end of their LF with redshift. (iii) Out to  $z\sim 0.5$ , the overall evolution of the galaxy population is dominated by changes seen in late-type spirals. The characteristic luminosity ( $L^*$ ) of these galaxies appears to brighten with redshift and there are signs of strong density evolution (a rapid increase in  $\phi^*$ ). These effects appear to be luminosity dependent so that the LF steepens at higher redshift. These trends are accompanied by a steep increase in the median [OII] equivalent width, implying a rapid increase in the star-formation rate with redshift at fixed luminosity—a given star-formation rate is found at higher redshift in galaxies of higher luminosity. We find that these conclusions are robust with respect to spectral classification errors and the luminosity function estimator. Finally, we briefly discuss the correlations between our ground-based dataset and a subset of 60 galaxies for which WFPC-2 images are now available from Hubble Space Telescope.

**Key words:** cosmology: observations – galaxies: evolution, large scale structure: galaxies – spectroscopy

## 1 INTRODUCTION

The Autofib Redshift Survey was introduced in the first paper in this series (Ellis et al. 1996, Paper I). It is an extensive compilation of over 1700 galaxy redshifts drawn from 53

\* Please direct correspondence to: Jeremy Heyl, Lick Observatory, University of California, Santa Cruz, CA 95064, USA

separate magnitude-limited slices spanning  $11.5 < b_J < 24.0$ . About half of the data has been published by our observing team during 1985–1994 in various papers (Peterson et al. 1985, Broadhurst, Ellis & Shanks 1988, Colless et al. 1990, 1993, Glazebrook et al. 1995a), and a further 1026 new redshifts have been secured in the intermediate magnitude range  $17 < b_J < 22$  using the Autofib fibre positioner on the 3.9m Anglo-Australian Telescope. The resulting dataset has the advantage of covering a wide luminosity range up to redshifts  $z \approx 0.75$ , and is thus ideally suited to studying the evolution of the galaxy luminosity function (LF). Details of the photometric selection, observing techniques, spectroscopic analysis and a comprehensive catalogue will be given in a subsequent paper (Paper III). We assume  $H_0 = 100 \text{ km s}^{-1} \text{ Mpc}^{-1}$  and  $q_0 = 0.5$  throughout.

The main goal of this paper is the determination of the evolution of the luminosity functions (LFs) by galaxy type. A number of studies at low redshift have investigated the LFs for different morphological types, for different colour classes, or for different degrees of star-formation activity (indicated by [OII] equivalent width). Among the most extensive of these studies are those of Binggeli, Sandage & Tammann (1988), Loveday et al. (1992), Marzke et al. (1994a) and Lin et al. (1996). This work has been directed toward understanding differences in the shape of the LF between the morphological types, and differences in the LFs of field and cluster galaxies.

In the last few years the size of deep redshift surveys has increased to the point where it has begun to be feasible to derive the evolution of the LF with redshift. Initial analyses were carried out by Eales (1993), Lonsdale & Chokshi (1993) and Treyer & Silk (1994) using the surveys of Peterson et al. (1985), Broadhurst, Ellis & Shanks (1988), Colless et al. (1990) and Cowie et al. (1991). These studies clearly indicated evolution of the LF with redshift (as had already been apparent from comparison of the galaxy number counts and redshift distributions with non-evolving models). However the size of these surveys was not large enough for the authors of the LF analyses to reach a clear consensus on the form of this evolution. Two new deep redshift surveys, the Canada-France Redshift Survey of 730 I-selected galaxies (Lilly et al. 1995) and our Autofib survey of over 1700 B-selected galaxies (Ellis et al. 1996; Paper I), have increased the sample sizes to the point that it is now possible not only to recover the evolution of the overall LF with redshift, but also to examine the evolution of the LF as a function of galaxy type.

Lilly et al. (1995) measured redshifts for a sample of galaxies with  $I < 22$  that reaches out to  $z \sim 1$ , obtaining LFs as function of both redshift and colour. They find that the LF evolution is strongly differential with colour, in the sense that the LF of red galaxies evolves little if at all out to  $z \sim 1$  while the blue population shows substantial evolution. Lilly et al.’s work probes to the highest redshifts yet explored, however their results are limited by the fact that they are working with a single magnitude-limited sample, so that

there is little overlap in the luminosity range spanned in different redshift ranges. Thus their results show different parts of the LF at different redshifts—the faint end at low redshifts, the knee at the median redshift of the survey, and the bright-end cutoff at  $z \sim 1$ —making it difficult to form a coherent picture of changes in the overall shape of the LF.

The Autofib survey addresses this problem, inherent in magnitude-limited samples, albeit at the expense of a lower mean redshift than that of CFRS, by combining several surveys with different magnitude limits, so that we cover a broad range of luminosities at all redshifts out to  $z \approx 0.75$  (see Figure 7 of Paper I). Another difference between this work and that of Lilly et al. is that whereas their sample is selected in the I band, and so emphasises galaxies dominated by older stellar populations, ours is B-selected, and so emphasises the galaxies with ongoing star-formation. Finally, whereas Lilly et al. use colour as the indicator of galaxy type (dividing their sample into red and blue classes), and whereas in Paper I we used [OII] equivalent width (comparing the LFs for galaxies with EWs greater and less than  $20 \text{ \AA}$ ), in this paper we use well-defined spectral types determined directly from our survey observations.

The results from the Autofib survey, whilst confirming the basic evolutionary trends identified by Lilly et al., are more suggestive of the possibility of two distinct populations. In particular, the evolving shape of the LF is more clearly seen, although to somewhat lower redshift than for CFRS, and the trend appears to be largely due to an increase in the volume density of  $0.1 - 1 L^*$  galaxies with strong [O II] emission. In Paper I, the LF was primarily explored as a function of redshift for the entire galaxy population. Here, we will utilise the spectral classifications to describe the evolution of galaxy luminosity function in greater detail. This is valuable because the spectra themselves offer a glimpse into details of the evolving components that cannot be gleaned from photometric and redshift data alone. As well as using the spectra to isolate different subsets of the data, we will coadd the spectra according to various selection criteria in order to see if the short-term star formation histories of distant galaxies, as revealed by diagnostic absorption lines, are different from those of their local contemporaries. This is appropriate because the Autofib spectra were obtained at unusually good spectral resolution for a faint sample ( $4-8 \text{ \AA}$  for  $b_J < 22$  and  $12 \text{ \AA}$  for  $22 < b_J < 24$  c.f.  $\approx 25 \text{ \AA}$  for the CFRS survey). For a limited subset of our fainter galaxies, we also briefly discuss Hubble Space Telescope (HST) images and correlations between morphology and photometric classifications.

Our secondary goal in this paper is to discuss these spectral classification techniques and also the extensions to LF estimation methods we have developed in order to deal with the very general nature of the survey sample and the extra degree of freedom represented by LFs which evolve with redshift. In Paper I these techniques were only briefly mentioned in discussing new results on both the faint end

of the local LF and the evolution of the overall galaxy LF since redshifts  $z \sim 0.75$ .

A plan of the paper follows. The spectral classification technique and the tests and simulations carried out to verify its precision and reliability are described in §2. Here we also discuss the correlation between photometric properties and HST morphologies. In §3 we review existing methods of LF estimation and derive extensions to two methods which allow both a clustering-insensitive direct estimate and a best-fit parametric model to be recovered for an evolving LF. These methods are tested and compared to the standard  $1/V_{\max}$  LF estimator in §4. In §5 we use the spectral classification and LF estimation techniques to determine the LFs as a function of both redshift and spectral type. These results, and their implications for the physical processes driving galaxy evolution, are discussed in §6. Our conclusions are presented in §7.

## 2 SPECTRAL CLASSIFICATION

In Paper I we stressed the importance of reliable  $k$ -corrections for the determination of the luminosity function over a wide redshift range. The lack of morphological classifications or colours for most of the surveys combined here means that traditional methods for estimating  $k$ -corrections cannot be uniformly applied. Only the DARS survey has been classified morphologically and only the LDSS-1 and LDSS-2 samples have  $b_j - r_f$  colours. Applying a mean  $k$ -correction or defining a new passband probably would not be fruitful as the galaxies span  $z \approx 0-1$ , so an extremely blue or red galaxy at high redshift would have its luminosity incorrectly estimated by over a magnitude, and using a mean-redshift could lead to errors nearly as large. Furthermore, the volume weighting implied would be even more uncertain. As a major goal of our survey is to estimate the LF as a function of spectral class, we need an approach that is both uniformly applicable and more reliable.

In principle, a  $k$ -correction could be ‘read’ directly from each flux-calibrated spectrum. In practice, the calibrations are too uncertain to allow the continuum shape of the spectra to be matched to a standard SED, as is demonstrated by a comparison of synthetic colours estimated from the spectra with those obtained from direct imaging. However, on smaller scales where spectral features can be measured, the data are considerably more reliable. Accordingly, we have developed a technique for classifying each galaxy spectrum in the survey which succeeds very well for but the most noisy spectra in the sample (those from the LDSS-1 and LDSS-2 surveys, for which we used the  $b_j - r_f$  colour to estimate the  $k$ -correction as in Colless et al. (1990)). This technique was briefly outlined in Paper I (§3.1); here it is described in detail and validated by a variety of tests.

### 2.1 The Cross-Correlation Method

To determine the spectral classification of each of the galaxies, we chose to cross-correlate the survey spectra against those of the Kennicutt (1992a, 1992b) spectral library. This library is highly appropriate for this task, not only in spectral resolution and wavelength range but also because the spectra represent the light integrated over a large portion of the local galaxies rather than of the central regions as is usually the case. The physical apertures involved are closely matched to those of Autofib and LDSS at their mean redshifts. The 2-arcsec effective aperture of these surveys corresponds to a physical size of  $2-8 h^{-1}$  kpc for redshifts between 0.1 and 1.1, well matched to the physical apertures used by Kennicutt (1992a, 1992b).

The cross-correlation technique works as follows. First both the Kennicutt template and survey spectra are smoothed on a scale of  $100\text{\AA}$  in the observer’s frame and these smoothed versions are subtracted yielding continuum-subtracted spectra. The spectra are then rebinned to  $2\text{\AA}$  per bin in the rest frame of the galaxy. The cross-correlation is defined to be

$$r = \frac{(\sum_i t_i o_i)^2}{\sum_i t_i^2 \sum_i o_i^2}. \quad (1)$$

where  $t_i$  and  $o_i$  are flux values in the  $2\text{\AA}$  bins in the template and observed spectra respectively. This procedure is similar to the method derived independently by Zaritsky, Zabludoff & Willick (1995). The survey spectrum is classed according to the morphological type of the template with which it most strongly correlates. Each Kennicutt template has an associated morphological classification given in Kennicutt (1992b). We find the King & Ellis (1985)  $k$ -correction that most closely corresponds to the Kennicutt classification, thus determining the  $k$ -correction for each galaxy over a range of redshifts for which it might be detected within the particular sub-survey given the apparent magnitude limits. We cannot use the Kennicutt data to directly calculate the  $b_j$   $k$ -corrections for  $z > 0.05$ , as they do not extend into the ultraviolet below  $3650\text{\AA}$ . On the other hand, the spectral energy distributions (SEDs) of Pence (1976) and King & Ellis (1985), which *do* extend into the UV, lack the small-scale spectral features that make the cross-correlation method possible. Kinney et al. (1993) have published a UV spectroscopic atlas of star-forming galaxies; unfortunately, the uncertainties in these data are too large in the wavelength range critical to estimating  $k$ -corrections ( $2800-3700\text{\AA}$ ) for this atlas to be useful for our purposes. Additionally, the IUE aperture is not well-matched to the distant population. By using the Kennicutt spectra as templates and the appropriate SEDs for the matched types, the  $k$ -correction can be readily found.

If one assumes that the noise level of the survey spectra is uniform with wavelength (a good assumption for the faintest spectra), the cross-correlation coefficients may be directly converted to a value of  $\chi^2$ :

**Table 1.** Success rates of the classification algorithm.

$\overline{S/N}$	Fluxed		Unfluxed	
	Template Correct	Type Correct	Template Correct	Type Correct
4.05	100%	100%	81%	84%
2.03	94%	94%	76%	83%
1.22	88%	90%	62%	72%
0.82	82%	86%	52%	68%

$$\chi^2 = \frac{1}{\sigma^2} \sum_i o_i^2 (1 - r) \quad (2)$$

Clearly the best template match will yield a minimum  $\chi^2$  value. In principle the  $\chi^2$  estimator enables the method to be made more sophisticated by including both a distribution of prior probabilities among the template galaxies and a list of those templates which are a near-equal match. This information may provide the basis of an error estimate for the  $k$ -correction of each galaxy, but is beyond the scope of this analysis, for which we used the ‘raw’  $r$ -values to determine the best-matching galaxy.

## 2.2 Simulated Tests

To verify the algorithm, we performed two series of tests. The first involved simulating the procedure using fluxed spectra. We randomly selected a Kennicutt spectrum, normalised it to a particular mean number of counts per bin and added a sky signal. Using the total count per bin, a random Gaussian deviate was chosen and this noise added prior to sky-subtraction. By repeating this process 100 times, we created an ensemble of test spectra of known signal/noise ratio in each pixel. Each of these spectra was processed as above and the success rate in returning the correct Kennicutt class was calculated. As Table 1 shows, the success rate is encouraging.

Next we tried to simulate the unfluxed spectra in the catalogue and also took into account the effect of varying the redshifts of the simulated spectra. Test spectra were generated as before except that each spectrum was multiplied by a response function which is zero outside 3600–7200Å and increases quadratically by a factor of two from the edge to the central wavelength. This response function can be blueshifted by a factor of  $\times 1$ –1.6 equivalent to a redshift of 0–0.6. Table 1 shows the success rates for these tests.

Figure 1 examines the results of the ‘unfluxed’ simulations in more detail. The most striking feature of the distribution is the diagonal ridge line which traces the correct classifications. Classes #2 (red ellipticals) and #4 (early spirals) are sometimes confused with class #3 (blue ellipticals). Furthermore, class #5 (intermediate spirals) are sometimes classified as class #3 (blue ellipticals) and as class #7 (star-bursting spirals). However, the overall agreement is excellent.

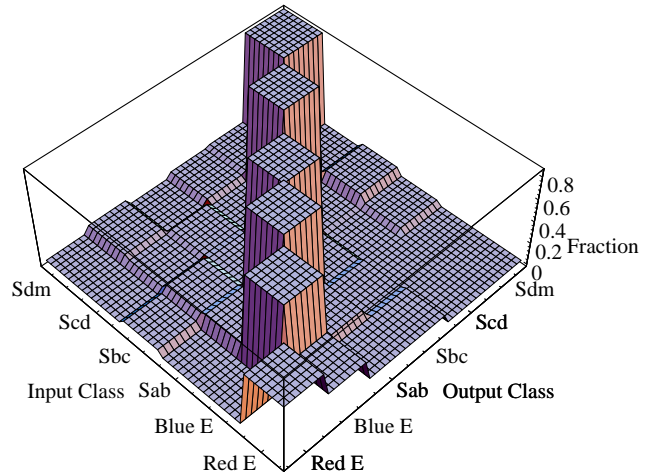


**Figure 1.** Input versus output classifications. The height of the surface represents the fraction of objects within each input class that were classified into each output. Red ellipticals and early spirals can be confused with blue ellipticals; and intermediate spirals can be confused both with earlier and later types.

As mentioned above, each  $k$ -correction class corresponds to several Kennicutt spectra, each with varying strengths of spectral features. Consequently, with the addition of noise, the spectra can be confused across a  $k$ -correction class. In the case of spectra for intermediate spirals which contain weak features of both earlier and later classes, the classification may be significantly in error.

Finally, we performed the blueshifting described above to simulate how observing galaxies at various redshifts through a fixed wavelength range can affect the success rate. Figure 2 shows that the error rate increases because a decreasing portion of a galaxy’s spectrum overlaps with the Kennicutt templates. We can only expect a satisfactory classification to  $z \simeq 0.6$ . For higher redshift galaxies in the LDSS-1 survey, and for all the LDSS-2 survey galaxies, we use colour to determine spectral class.

## 2.3 Sample Spectra

Figures 3 and 4 illustrate examples of the spectral classification technique. In each case the lower curve is the observed spectrum and the middle curve is the Kennicutt spectrum selected as the closest match. The continuum has been subtracted from both spectra as described earlier and the observed spectrum has been smoothed further to accentuate the features. The upper curve is the product of the two spectra smoothed over 20 bins to show which features contribute most strongly to the total cross-correlation.

Examining the brighter survey galaxies (Figure 3) there is strong correspondence between the observed spectra and the best templates. Intermediate-type galaxies are the most challenging as seen from the middle panel of Figure 3. How-

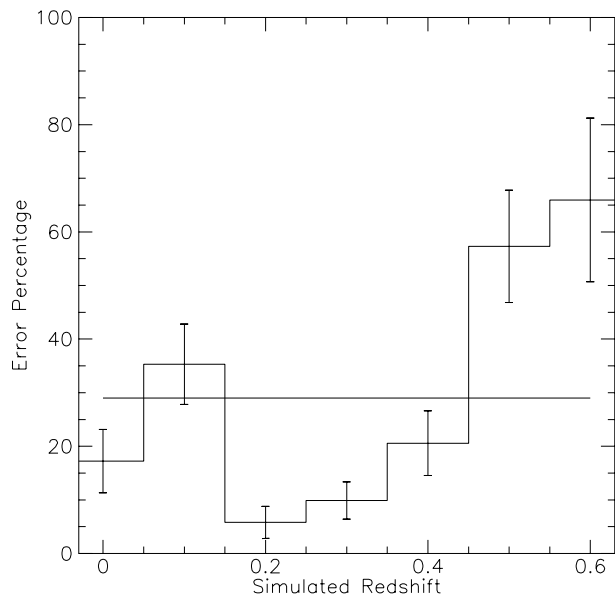


**Figure 2.** Classification error rate as a function of redshift. The error increases markedly with redshift, as the identifying features of the spectra are lost off the red end of our simulated spectrograph. The horizontal line is the mean error rate of the various tests: 29%.

ever even with faint galaxies (Figure 4) the algorithm performs well. However, the limited overlap at higher redshifts is a stumbling block (as predicted by Figure 2). Presently there is no equivalent spectroscopic atlas covering near-ultraviolet wavelengths, and in any case there are few strong features blueward of the [OII] emission line that would be helpful. For more distant sources, the most promising option would be to extend the observing window redwards utilising night sky suppression techniques to limit the deleterious effects of the OH emission.

## 2.4 Tests with Real Spectra

A subset of the galaxies in the catalogue have  $b_J - r_F$  colours and this provide an independent test of the classification algorithm. The LDSS-1 galaxies (Colless et al. 1990) lie within  $21 < B < 22.5$  and are amongst the faintest in the survey.

We use a two-stage test: the correlation of observed colour against  $k$ -correction class and correlation of ‘predicted’ colour against observed colour. We calculate the  $b_J - r_F$  colour in the observer’s frame by using the classification of each LDSS spectrum using our method and then determining the colour of the appropriate SED at the redshift of the galaxy. Figure 5 shows the results of both these tests.

The trend of colour versus class (first panel) exhibits a large spread which could arise from observing errors, colour

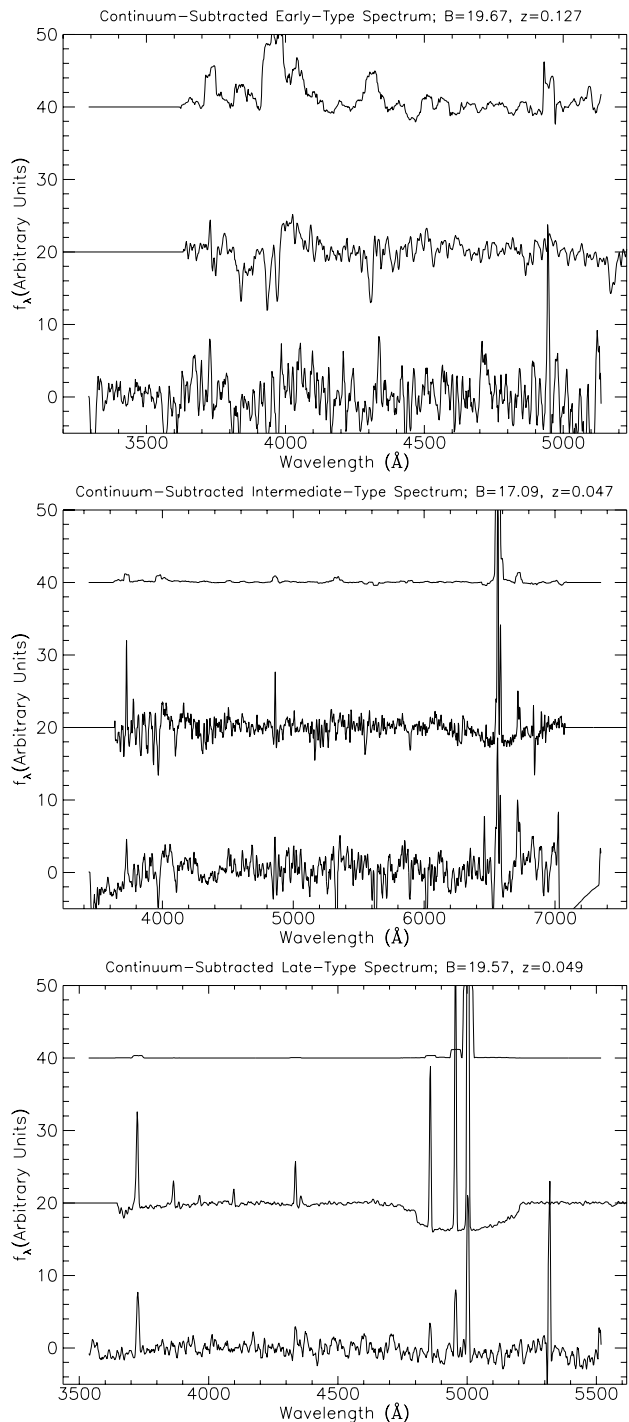


**Figure 3.** Classifying bright spectra. Three continuum-subtracted spectra selected from the bright section of the Autofib survey—from top to bottom, an early-type galaxy ( $B=19.67$ ,  $z=0.127$ ), an intermediate-type galaxy ( $B=17.09$ ,  $z=0.047$ ) and a late-type galaxy ( $B=19.57$ ,  $z=0.049$ ). The lower curve in each panel traces the the observed spectrum after the continuum has been subtracted, best-fitting (continuum-subtracted) spectrum from the Kennicutt atlas. The middle curve is best-fitting (continuum-subtracted) spectrum from the Kennicutt atlas, and the upper is the cross-correlation contribution as a function of wavelength.

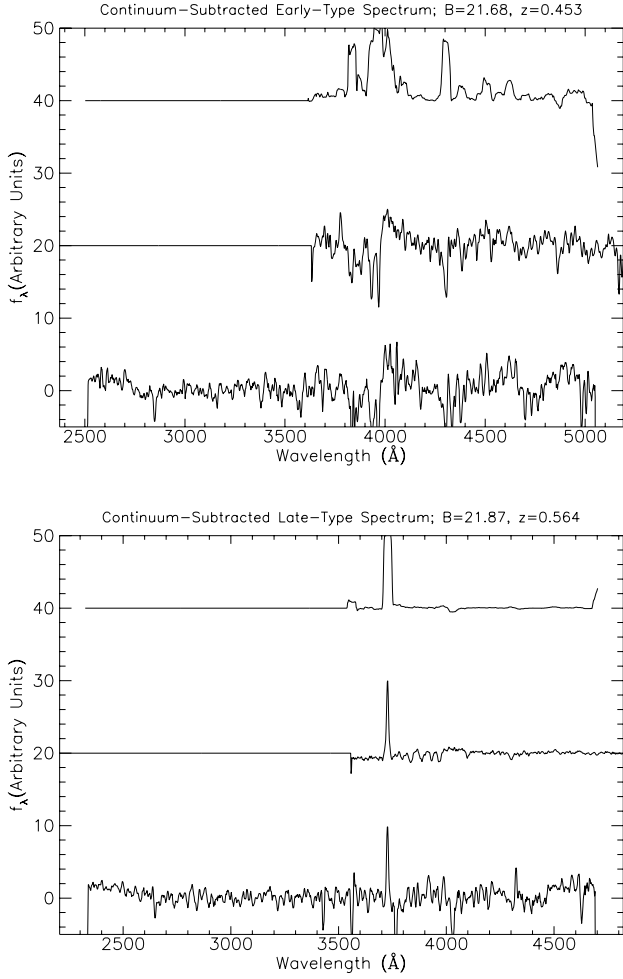


**Figure 4.** Classifying faint spectra. Two spectra selected from the faint section of the Autofib survey. The upper panel is an early-type galaxy ( $B=21.68$ ,  $z=0.453$ ). The lower panel is a late-type galaxy ( $B=21.87$ ,  $z=0.564$ ). The arrangement is as in the previous figure.

corrections and misclassifications. The second panel shows the predicted colour against the observed colour thereby removing the effect of redshift. Although the trend is remarkably good the mean-absolute error is approximately 0.4 mag. Budgeting the errors for this multistage process is difficult, as they arise in several places. The  $b_J$  and  $r_F$  magnitudes each have on average an uncertainty of 0.1 mag leading to a total error in the colour of 0.15 mag. Furthermore, a few galaxies have colours bluer than any of the  $k$ -correction SEDs; this is worrisome, but the effect is small and limited to only a few galaxies.

The remaining spread of approximately 0.3 mag may be due to either the variance of the intrinsic colours of galaxies within a given spectral class (deVaucouleurs 1977) or

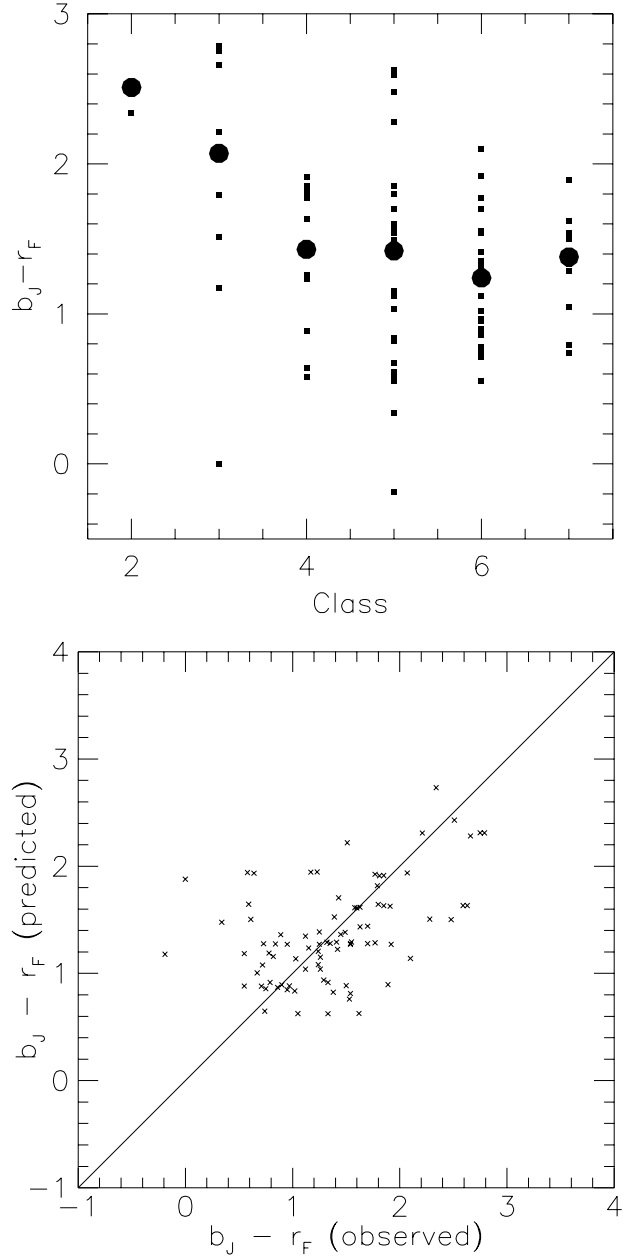


**Figure 5.** Results for LDSS-1 spectra. The upper panel depicts the spread in observed  $b_J - r_F$  colour for the galaxies in the LDSS-1 survey against the  $k$ -correction classification. Each small square represents a single galaxy. The large circles show the trend in the median colour for each class. The lower panel shows colour predicted from the  $k$ -correction classification at the redshift of each galaxy against the observed colour of the galaxy. Each square represents a galaxy in the survey.

to misclassifications. Although it depends on  $k$ -correction class, the error in the  $k$ -correction is approximately 1.5 times greater than the colour error, so if all the spread in this plot were due to misclassifications, the  $k$ -corrections for these galaxies would have an RMS error of 0.6 mag. The LDSS-1 data are the most noisy of the survey and we expect some scatter in the intrinsic galaxy colours; consequently, we expect the mean misclassification rate and the  $k$ -correction error to be much lower over the entire survey and an unimportant source of error in the luminosity function estimates.

## 2.5 Testing with HST

Given the limited usefulness of comparing spectral classifications with those based on broad band colours, it is interesting to compare both classifications with those based on morphologies derived from the Hubble Space Telescope (HST) images. For the brighter redshift surveys (Peterson et al. 1985, Loveday et al. 1992)  $k$ -corrections have normally been assigned on the basis of a Hubble type determined from visual inspection and thus it is important, where possible, to examine the correlation between Hubble type and the diagnostics we have employed in this work to classify our spectra and faint galaxies.

As part of a major programme to morphologically resolve the faint field population, we have imaged about 80 galaxies in the fields sampled by our survey with  $21 < b_J < 24$  with the HST WFPC-2. Typical integration times were 4-6 orbits in the F814W filter. Of these 80, 64 have spectra and redshifts as part of the Autofib survey. Most of these are drawn from the LDSS-2 catalogue although a few LDSS-1 and fibre sample galaxies were also observed. At these apparent magnitudes the spectra are generally too faint or highly redshifted for the cross-correlation technique to be a reliable classifier (c.f. Figure 2) and the bulk of the classifications are thus based on  $b_J$ - $r_F$  colours.

Each of the 64 galaxies has been assigned a morphological type by one of us [RSE] according to the morphological scheme introduced for analyses of the Medium Deep Survey (Glazebrook et al. 1995b) and Hubble Deep Field (Abraham et al. 1996). Briefly, galaxies were classified visually on the F814W image according to a scheme whose internal resolution adapts to the varying quality and size of the individual images. Although the scheme has 12 one-dimensional classes, in this comparison we have collated the data into 5 broader classes, namely stellar/compact, spheroidal, early/intermediate spiral, late-type spiral/Irregular, merger/unclassified. In the following we examine how well these HST morphologies correlate with the classes used in the rest of the paper noting that these are, largely, based on colour.

Figure 6 shows the  $b_J$ - $r_F$  colour-redshift relation with each datapoint denoted according to its HST morphology, as well as a direct comparison of the HST morphological type with the  $k$ -correction class based on the broad-band colours

or spectroscopic cross-correlation. In these plots 3 QSOs in the HST sample have been removed but objects which defied classification in one or both schemes have been included.

As before, recognising that morphology and colour/spectral class do not perfectly align even with high signal/noise local data, we can consider the agreement to be satisfactory; 52% of the HST-classed galaxies lie on the ridge line, sharing identical classifications. The largest systematic deviation appears to be with the morphologically-defined spheroidal galaxies where a significant proportion have spectral or photometric properties which class them as early-type spirals. On closer inspection these sources include galaxies which appear to lie at the boundary of the S0 and early-type spiral region. However, as discussed later, there do appear to be a number of cases where HST-classed ellipticals have slightly bluer colours than expected and this is accompanied by [O II] emission, so the blurring of classes in the spheroidal/early-type spiral region is partially a physical effect.

More extreme misclassifications than those which transfer data to adjacent bins are rarer and, upon inspection, easier to understand. For example, there are quite a few compact objects which are HII-galaxies with extremely blue colours and spectra indicative of late-type spirals. Under our simple morphological scheme, these are binned with the ellipticals since this classification boundary for distant objects is difficult to discern. There is also one compact red object with an emission line.

## 3 LUMINOSITY FUNCTION ESTIMATORS

Once the luminosities of survey galaxies have been determined (see § 3.2 of Paper I), the next logical step in our analysis is to construct the luminosity function as a function of class. A number of possible LF estimators have been discussed in the literature (see reviews by Felten (1976), Efsthathiou, Ellis & Peterson (1988)). In the particular case of the Autofib survey, we are interested in an estimator which is well-suited to the deep pencil-beam nature of the survey which may imply greater large scale structure fluctuations than would be the case for panoramic all-sky surveys.

In Paper I, we presented LF results based on a simple estimator, the  $1/V_{\max}$  method (Schmidt 1968), arguing that although the redshift distribution in individual pencil beams may suggest large departures from that expected for a homogeneous distribution, the large number of individual beams (53 in 9 widely distributed regions) should minimise such difficulties. Here we will explore this assumption more carefully by developing a modified version of the Step-Wise Maximum-Likelihood (SWML) method. That method, and its derivatives, has become a popular tool to overcome the effects of fluctuations by assuming the LF has the same *shape* across all density fluctuations in the survey. Although useful in local surveys, as we are interested in examining potential evolutionary changes in the LF this restriction is unacceptable.

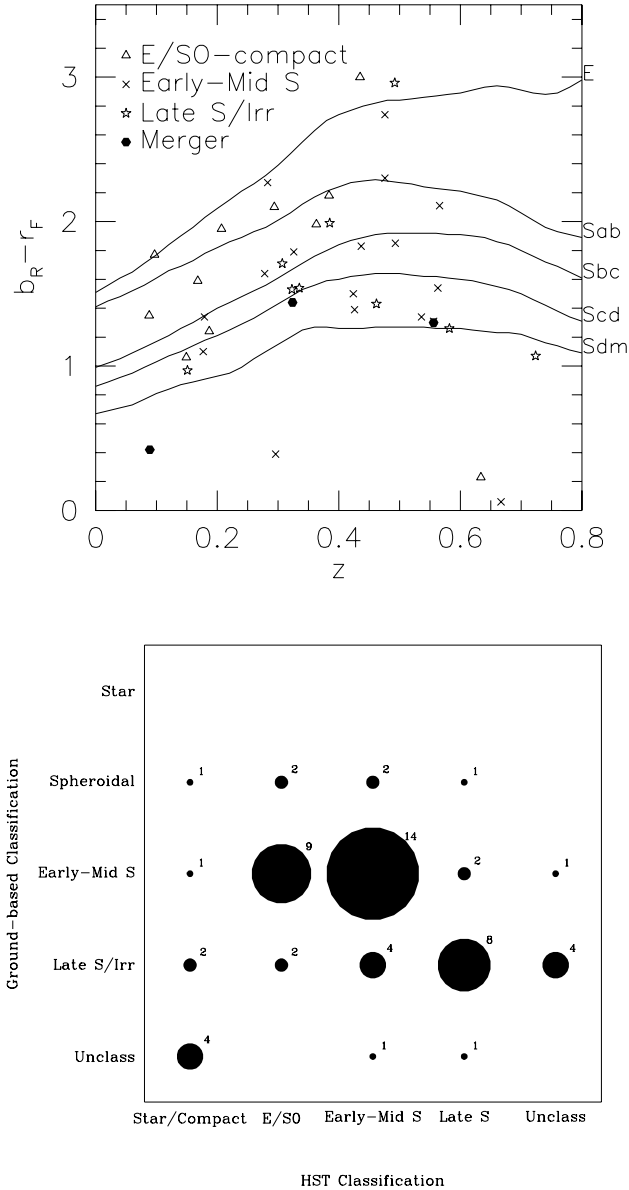


**Figure 6.** Correlations with HST morphology. The upper panel shows the observed  $b_J - r_F$  colour-redshift relation for 55 galaxies in the LDSS-1 and LDSS-2 surveys. Different symbols have been used according to the 5 HST morphologies discussed in the text (see inset). The curves represent the expected trends for the adopted set of  $k$ -corrections. The lower panel shows a direct comparison between HST morphology and photometric/spectroscopic class including those sources which defied classification in one or both systems. The area of each circle is proportional to the sample size in each category and is indicated numerically.

able. In the following sections we derive and compare various alternate methods for estimating the LF which do not impose this constraint.

### 3.1 The $1/V_{\max}$ Method

We begin by briefly reviewing the  $1/V_{\max}$  method used in Paper I. The first step in this method is the calculation of the total volume within which the object could have been observed. In a single magnitude-limited survey (see § 3.2 of Paper I) :

$$V_{\max} = \frac{c}{H_0} A \int_{z_{\min}}^{z_{\max}} \frac{d_L^2 dz}{(1+z)^3 \sqrt{1+2q_0 z}} \quad (3)$$

where  $z_{\min}$  and  $z_{\max}$  are the minimum and maximum redshifts from which the object could have been observed in the survey considering the distance modulus and  $k$ -correction.  $A$  is the area of sky surveyed in steradians. In its simplest form, the luminosity function is obtained by collecting the sources in bins of constant magnitude and summing the  $(V_{\max})^{-1}$  values in each group.

Avni & Bahcall (1980) describe how to combine more than one sample coherently in a  $V/V_{\max}$  analysis. The new variable, denoted  $V_a$  is simply the sum of  $V_{\max}$  over all the surveys in which the object could have been observed. Finally, Eales (1993) describes how to use this variable to construct the luminosity function as a function of redshift. The analysis proceeds according to Schmidt's method with the exception that the data is also binned in redshift. Here  $z_{\min}$  is the minimum redshift at which the object could have been observed in the magnitude-limited sample and be in the redshift range of interest. The method works similarly for the maximum redshift.

As mentioned, these variants of the traditional  $1/V_{\max}$  estimator are each affected by the presence of clustering in the sample. Clustering will lead to a poor estimate of the faint-end slope of the luminosity function.

### 3.2 Clustering-Insensitive Methods

Several authors have introduced estimators, which although slightly biased, reduce the effects of clustering on the resulting LFs. Each of these techniques attempts to maximise the likelihood of observing a particular set of galaxies by varying parameters of the luminosity and completeness functions. The methods differ in the way the assumed probability of observing a particular galaxy is calculated.

Adopting Poisson statistics is an obvious way of proceeding. This assumption was first applied to the analysis of quasar samples (Marshall et al. 1983) and later recast to analyse the CfA redshift survey (Cholomiewski 1986). The probability of observing  $k$  galaxies in the interval  $dMdz$  in an area of sky  $d\Omega$  is

$$P_k = e^{-\lambda} \frac{\lambda^k}{k!} . \quad (4)$$



where

$$\lambda = \frac{1}{n} \phi(M) \rho(z) dM dz d\Omega \quad (5)$$

and  $n$  is the average number density of the survey. By binning  $\phi(M)$  and  $\rho(z)$ , these two functions may be estimated without assuming particular forms. The only task that remains is to maximise the total probability of the survey (the product of all the  $P_k$  in each of the bins) while varying the values of  $\phi(M)$  and  $\rho(z)$ .

The C-method (Lynden-Bell 1971) adopts a different approach. By considering the plane of redshift *versus* absolute magnitude, this method uses the fact that the ratio of the number of galaxies observed between  $L$  and  $L+dL$  to the number brighter than  $L$  is proportional to the ratio of the number of galaxies actually in the field in this range to those brighter than  $L$  multiplied by a weighting factor to account for the differing volumes sampled. The method generates a cumulative luminosity function without normalisation. The differential luminosity function may be derived by fitting an appropriate model.

The STY method (Sandage, Tammann & Yahil 1979) twists this plane around. It examines the probability that a galaxy observed at a redshift  $z_0$  is brighter than  $M$ :

$$P(M, z_0) = \frac{\int_{-\infty}^M \phi(M') D(z_0) f(m') dM'}{\int_{-\infty}^{\infty} \phi(M') D(z_0) f(m') dM'} \quad (6)$$

where  $f(m)$  is the completeness of the survey at apparent magnitude  $m$  and  $D(z)$  is the density of galaxies at redshift  $z$  divided by the mean density of galaxies ( $\bar{\rho}$ ). Taking the derivative of this equation with respect to  $M$  yields the probability density for finding a galaxy with absolute magnitude  $M$  in a magnitude-limited survey. This probability is directly proportional to the density of galaxies with that apparent magnitude and inversely proportional to that which could have been observed at that particular redshift,

$$p_k \propto \phi(M_k) \left/ \int_{M_{\text{faint}}(z_k)}^{M_{\text{bright}}(z_k)} \phi(M') dM' \right. \quad (7)$$

Here we have replaced the function  $f(m')$  with a function that is zero outside the magnitude limits of the survey and unity within (i.e. assuming that the survey is 100% complete). As the redshift of the galaxy is fixed, the discontinuities in  $f(m')$  correspond with the range of absolute magnitudes beyond which no galaxies at this redshift could have been observed.

Finally, the Step-Wise Maximum-Likelihood method follows from equation 7 (Efstathiou, Ellis & Peterson 1988). Our modification of the SWML method (SSWML) complements Cholońiewski's method, but for a different statistical model.

### 3.3 Deriving the SSWML Method

The aforementioned clustering-insensitive methods by design probe the LF as a function of luminosity only. To understand the evolution of the LF with redshift, this restriction must be removed. Here we will derive two new methods that avoid this restriction. They are based on, respectively, the STY and SWML methods. Our generalisations of the locally-valid estimators will be denoted with a prefixed 'S' for spatial, i.e. SSTY and SSWML respectively.

In the derivation, it becomes apparent that these generalisations provide some additional rewards. For example, they provide a straightforward prescription to combine various surveys coherently and to determine the absolute normalisation.

The derivation of the SSWML method begins with equation 6 of the STY method, modified by two generalisations:

- $\rho(z, M) \neq \bar{\rho} D(z) \phi(M)$  (i.e. luminosity and density evolution are separately permitted), and
- $f(m) = \Omega(m)$ , where  $\Omega(m)$  is the area of sky sampled at apparent magnitude  $m$ , accounting for sampling rate and mean completeness.

These two generalisations will allow the determination of the LF as a function of redshift (as in Cholońiewski 1986) and the use of many surveys in a single coherent determination of the luminosity function.

The relevant probability is that of finding a galaxy in the survey brighter than  $M$  and closer than  $z$ :

$$P(M, z) = \frac{\int_0^z \int_{-\infty}^M \rho(z', M') \Omega(m') \frac{dV}{dz'} dM' dz'}{\int_0^{\infty} \int_{-\infty}^{\infty} \rho(z', M') \Omega(m') \frac{dV}{dz'} dM' dz'} \quad (8)$$

Again, taking the derivative of this equation yields the probability density:

$$p_k = \frac{\partial^2 P(M, Z)}{\partial M \partial z} \propto \rho(z_k, M_k) \left/ \int_0^{\infty} \int_{-\infty}^{\infty} \rho(z', M') \Omega(m') \frac{dV}{dz'} dM' dz' \right. \quad (9)$$

where  $\Omega(m)$  is the solid angle sampled at the apparent magnitude  $m$ , and  $m$  is the apparent magnitude corresponding to  $M$  and  $z$  considering the distance modulus and effects of the  $k$ -correction. Consequently  $m$  may best be written  $m(z, M; c_k)$  where  $c_k$  is the  $k$ -correction class of galaxy  $k$ . This equation forms the basis of the SSTY method.

Figure 7 compares Equations 7 and 9 on the absolute magnitude *versus* redshift plane. The lower double integral is simply the number of galaxies that one would expect to observe in a combined survey given a LF. If the function  $\Omega(m)$  is simply a series of steps (as in Figure 7), there is only one  $k$ -correction class, and the trial LF is integrable at a given redshift (like an evolving Schechter function), the

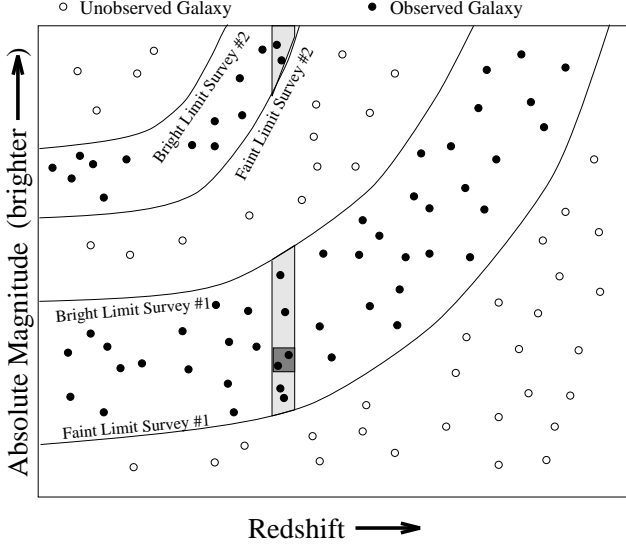


**Figure 7.** Geometric comparison of the STY and SSTY methods. In the STY method, the probability of observing a galaxy is the ratio of the number of galaxies at the galaxy's absolute magnitude (the dark-shaded region) to the total number that could have been observed within the magnitude limits at the same redshift as the observed galaxy (the light-shaded region). The extension to the SSTY technique is straightforward. The probability of observing a galaxy at a particular redshift is the ratio of the density of galaxies at the observed redshift and absolute magnitude (again the dark-shaded region) to the total number of galaxies that could have been observed at any redshift (the region enclosed by the magnitude limits).

integral may be most efficiently calculated as

$$N_{\text{gal}}^{\text{pred}} = \int_0^\infty \sum_j \Omega_j \int_{B_{j,\min}}^{B_{j,\max}} \frac{dV}{dz} dm' dz' \times \rho(z', m' - d_{\text{modulus}}(z) - k(z)) \quad (10)$$

where the sum is over the subsurveys and the  $j$ th survey samples  $\Omega_j$  steradians in an apparent magnitude range from  $B_{j,\min}$  to  $B_{j,\max}$ . Although the function  $\rho(z, M)$  may not be separable, if the evolution of the LF is posed as an evolution of separable Schechter parameters,  $\rho(z, M)$  takes the form of an integrable Schechter function at all redshifts.

Although now complex, if we reinstate the assumption that the density is separable and that we have a single magnitude-limited sample, this formula reduces to Equation 7:

$$p_k \propto n(z_k) \phi(M_k) \left/ \int_0^\infty n(z) \frac{dV}{dz} \int_0^\infty \phi(M) \Omega(m) dM' dz' \right. \quad (11)$$

We can calculate  $\Omega(m)$  for  $z_k$

$$\Omega(m) = \begin{cases} \Omega & \text{if } M_{\text{faint}}(z_k) \leq M \leq M_{\text{bright}}(z_k) \\ 0 & \text{otherwise} \end{cases} \quad (12)$$

Since we seek an estimator for  $\phi(M)$  which is assumed con-

stant everywhere, we can choose to perform the latter integral at the redshift of the observed galaxy ( $z_k$ ), yielding

$$p_k \propto n(z_k) \phi(M_k) \left/ \int_0^\infty n(z) \Omega \frac{dV}{dz} dz \int_{M_{\text{faint}}(z_k)}^{M_{\text{bright}}(z_k)} \phi(M) dM \right. \quad (13)$$

which reduces to the STY result.

We now proceed in the spirit of the SWML (Efstathiou, Ellis & Peterson 1988) method and assume that  $\rho(z, M)$  is defined for a two-dimensional array of steps in both redshift and luminosity,

$$\rho(z, M) \equiv \sum_{ij} W(z - z_i, M - M_j) \rho_{ij} \quad (14)$$

where

$$W(z, M) = \begin{cases} 1 & \text{if } -\Delta z/2 \leq z \leq \Delta z/2 \text{ and } -\Delta M/2 \leq M \leq \Delta M/2 \\ 0 & \text{otherwise} \end{cases} \quad (15)$$

Substituting this relation into the formula for  $p_k$  gives

$$p_k \propto \sum_{ij} W(z_k - z_i, M_k - M_j) \rho_{ij} \left/ \sum_{ij} \rho_{ij} \int_{z_i - \Delta z/2}^{z_i + \Delta z/2} \int_{M_j - \Delta M/2}^{M_j + \Delta M/2} \Omega(m) \frac{dV}{dz} dM dz \right. \quad (16)$$

Next we calculate the logarithm of  $p_k$

$$\ln p_k = \sum_{ij} W(z_k - z_i, M_k - M_j) \ln \rho_{ij} - \ln I_k \quad (17)$$

where we have replaced the denominator with  $I_k$ . The subscript  $k$  is retained because the value of the integral depends on the  $k$ -correction for the particular galaxy observed through  $\Omega(m(z, M; c_k))$ .

The likelihood of observing the entire survey is the product of the likelihoods for each galaxy

$$P_{\text{survey}} = \prod_k p_k, \quad (18)$$

and taking the logarithm,

$$\ln P_{\text{survey}} = \sum_k \ln p_k. \quad (19)$$

Because we would like to maximise the survey likelihood, we examine the derivative with respect to  $\rho_{pq}$  and search for stationary points:

$$\frac{d \ln P_{\text{survey}}}{d \rho_{pq}} = \sum_k \frac{d \ln p_k}{d \rho_{pq}} = 0. \quad (20)$$

Differentiating Equation 17,

$$\frac{d \ln p_k}{d \rho_{pq}} = \frac{W(z_k - z_p, M_k - M_q)}{\rho_{pq}} - \frac{1}{I_k} \frac{d I_k}{d \rho_{pq}}. \quad (21)$$

Referring to Equation 16, we see that

$$\frac{dI_k}{d\rho_{pq}} = \int_{z_p - \Delta z/2}^{z_p + \Delta z/2} \int_{M_q - \Delta M/2}^{M_q + \Delta M/2} \Omega(m) \frac{dV}{dz} dM dz \quad (22)$$

and

$$I_k = \sum_{pq} \rho_{pq} \frac{dI_k}{d\rho_{pq}} \quad (23)$$

Summing over the derivatives (Equation 21) gives

$$\frac{d \ln P_{\text{survey}}}{d\rho_{pq}} = \sum_k \left( \frac{1}{\rho_{pq}} W(z_k - z_p, M_k - M_q) - \frac{1}{I_k} \frac{dI_k}{d\rho_{pq}} \right). \quad (24)$$

and setting this to zero yields

$$\rho_{pq} = \frac{\sum_k W(z_k - z_p, M_k - M_q)}{\sum_k \left\{ dI_k/d\rho_{pq} / \sum_{ij} \rho_{ij} dI_k/d\rho_{ij} \right\}} \quad (25)$$

which is familiar in form to the SWML result,

$$\phi_q \Delta M = \frac{\sum_k W(M_k - M_q)}{\sum_k \left\{ H[M_q - M_{\text{faint}(z_k)}] / \sum_j \phi_j \Delta M H[M_j - M_{\text{faint}(z_k)}] \right\}} \quad (26)$$

since we can identify  $I_k$  with the sum over  $j$  in the denominator and  $dI/d\rho_{pq}$  with  $H[M_q - M_{\text{faint}(z_i)}]$  also in the denominator.

Calculating the values in the denominator of Equation 25 is less straightforward than in the SWML method, but Equations 22 and 23 show that this denominator is a function of the  $\rho_{pq}$ , the  $k$ -correction class of galaxy  $k$ , the cosmology (through  $dV/dz$  and the distance modulus), and the details of the survey (through  $\Omega(m)$ ). Therefore we can calculate the values of the  $dI_k/d\rho_{pq}$  for each  $k$ -correction class before beginning the iterative solution to Equation 25.

Furthermore, since the integrals  $I_k$  are over volume, it is straightforward to calculate the total number of galaxies expected given the current values of  $\rho_{ij}$ ,

$$n_{\text{gal}}^{\text{pred}} = \sum_{ijk} f_k \rho_{ij} \frac{dI_k}{d\rho_{ij}} \quad (27)$$

where  $f_k$  is the fraction of the galaxies observed in each  $k$ -correction class. All  $\rho_{pq}$  can then be normalised so that Equation 27 yields the number of catalogue galaxies. The normalisation can be done either at each iteration by multiplying the right-hand side of Equation 25 by  $n_{\text{gal}}^{\text{observed}}/n_{\text{gal}}^{\text{pred}}$ , or by multiplying this ratio after the final iteration. The algorithm converges more quickly (two or three iterations) if the normalisation is performed at each step.

Errors may be estimated following procedures discussed

by Saunders et al. 1990:

$$\begin{aligned} \sigma(\log \rho_{pq}) &= (\ln 10)^{-1} \sigma(\ln \rho_{pq}) \\ &= (\ln 10)^{-1} \left( \frac{\partial^2 \ln P_{\text{survey}}}{(\partial \ln \rho_{pq})^2} \right)^{-1/2} \end{aligned} \quad (28)$$

$$\begin{aligned} &= (\ln 10)^{-1} \times \\ &\quad \left[ \sum_k \left\{ W(z_k - z_p, M_k - M_q) \right. \right. \\ &\quad \left. \left. - \left( \rho_{pq} \frac{dI_k}{d\rho_{pq}} / \sum_{ij} \rho_{ij} \frac{dI_k}{d\rho_{ij}} \right)^2 \right\} \right]^{-1/2}. \end{aligned} \quad (29)$$

Additionally, it is straightforward to estimate upper limits for bins in which no galaxies are observed.

$$\rho_{pq}^{\text{upper}} = \frac{1/2}{\sum_k \left\{ dI_k/d\rho_{pq} / \sum_{ij} \rho_{ij} dI_k/d\rho_{ij} \right\}} \quad (30)$$

In this derivation,  $\Omega(m)$  includes several important factors. The simplest way to define  $\Omega(m)$  is to calculate the area surveyed in each subcatalogue and then multiply this area by the sampling rate and completeness.  $\Omega(m)$  then represents a series of steps with a jump at the bright and faint limits of each subcatalogue. However, we can generalise this in two ways. Firstly, since we explicitly calculated  $dI_k/d\rho_{ij}$  for each galaxy type, we can introduce completeness as a function of  $k$ -correction type by defining various  $\Omega_k(m)$ . Secondly, we can calculate the completeness rate within a subcatalogue as a function of apparent magnitude and account for this in obtaining  $\Omega(m)$  or  $\Omega_k(m)$ . These two generalisations make this technique an extremely versatile tool in analysing galaxy catalogues.

## 4 TESTS AND COMPARISONS

To test the  $1/V_{\text{max}}$  and SSWML methods in a large sample like the composite DARS, AUTOFIB and LDSS-1/2 surveys, we generated a random galaxy catalogue from a Schechter function (Loveday et al. 1992). In the first test 1800 galaxies were selected in a standard cosmology, 300 from each of the following magnitude ranges: 11.0–17.3, 17.0–19.7, 19.7–20.5, 20.3–20.8, 20.8–22.5, and 22.5–24.0. All the galaxies were assigned zero  $k$ -correction and the density of galaxies was doubled beyond a redshift of 0.2 to crudely simulate density evolution.

Figure 8 illustrates the results of this simulation. It can be seen that the two methods generate nearly identical LFs, although the SSWML method produces smoother results. The bootstrap errors of the  $1/V_{\text{max}}$  method agree remarkably well with errors derived for the maximum likelihood technique. Although in principle the SSWML technique has the additional advantage of determining upper limits which further constrain the evolution of the faint-end slope, these

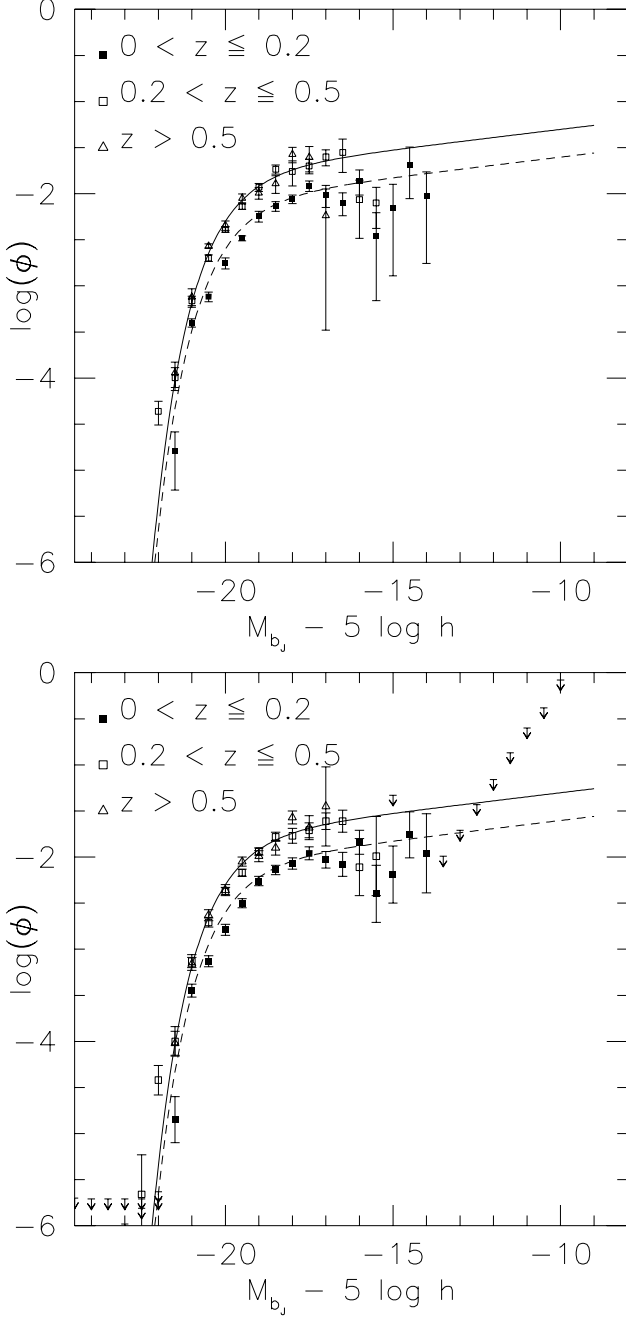


**Figure 8.** Test catalogue of 1800 galaxies. The upper panel depicts the results of the  $1/V_{\max}$  analysis on the random galaxy catalogue and the lower panel shows the results of the SSWML method. In each panel the lower curve is the nearby ( $z < 0.2$ ) luminosity function, and the upper is the distant one. The errorbars for the  $1/V_{\max}$  method are generated using a bootstrap technique, while the errors and upper limits for the SSWML are determined as described in the text.

upper limits increase with a slope of  $\alpha = -2$  and so in practice are not very interesting much fainter than the observed points.

To test whether either of the techniques are biased and to find an external error measurement, we generated an ensemble of ten catalogues derived from the same evolving LF as depicted in Figure 8. Each catalogue contained 1,800 objects sampled as in the previous test. We found that neither method is systematically biased relative to the input luminosity function and that the internal error estimates satisfactorily approximate the scatter of the luminosity functions derived for the ensemble.

#### 4.1 Sensitivity to Clustering

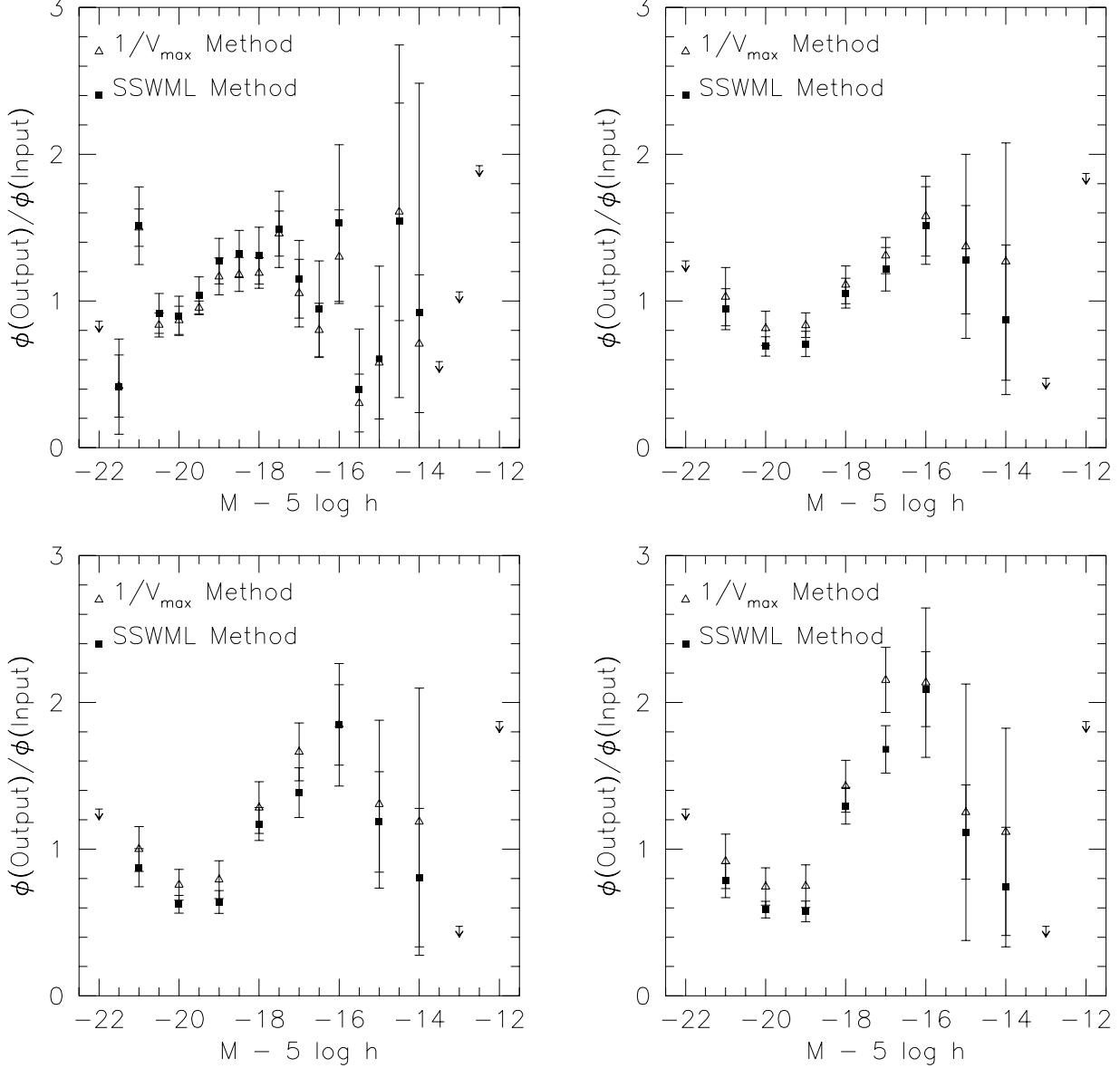
To test the sensitivity of the algorithms to clustering, three additional galaxy catalogues were generated with an overdensity of galaxies at a redshift of 0.05 with a dispersion in redshift of 0.003 in one of the fields in the 17.0–19.7 survey. The ‘cluster’ LFs were assumed identical to that in the field, but were normalised such that a set fraction of the 300 galaxies in the 17.0–19.7 magnitude range were in the cluster. The three surveys had clustered fractions of 45%, 65% and 85%.

Figure 9 shows the results of this simulation for the most populous cluster for a variety of bin widths. The  $1/V_{\max}$  and the narrowly-binned SSWML methods both over-predict the faint end of the LF. However, as the bin width of the SSWML method is increased, the over-prediction decreases. The ‘smooth binning’ technique uses two SSWML calculations with bins of two magnitudes, shifted by one magnitude relative to each other. This achieves the closest results to the input LF.

Figure 10 compares the LFs derived from the 3 clustered catalogues and the unclustered catalogue. Both the SSWML and  $1/V_{\max}$  methods derive successively steeper LFs as the strength of the clustering is increased, whereas the SSWML estimator is clearly less affected. In summary, these tests reveal the superiority of the SSWML method in surveys affected by clustering.

#### 4.2 The Relation between the Methods

Figure 9 reveals an interesting correspondence between the  $1/V_{\max}$  and the maximum-likelihood technique. It appears that the smaller the SSWML bins, the closer it approximates the  $1/V_{\max}$  method. Looking back to Equation 25, the sum over the  $k$  objects in the survey in the numerator may be replaced with  $n_{pq}$ , the number of objects in the appropriate bin. Furthermore, consider the case where there is only one type of galaxy. This is not a restrictive assumption, as one could split the surveyed galaxies by type, calculate the LF of each type independently prior to addition. These two approaches result in



**Figure 10.** Luminosity functions ( $0.02 \leq z < 0.15$ ) as a function of clustering. The top-left panel has no clustered galaxies. In the top-right panel, 45% of the galaxies in the B=17–19.7 subcatalogue are in a cluster at  $z=0.05$ . In the lower panels 65% (left) and 85% (right) of these galaxies are clustered.

$$\rho_{pq} = \frac{n_{pq}}{n_{\text{gal}}^{\text{observed}}} \frac{\sum_{ij} \rho_{ij} dI/d\rho_{ij}}{dI/d\rho_{pq}} \quad (31)$$

where the sum over  $k$  has been replaced by a multiplication. Referring to Equation 27, the sum in the numerator may be replaced with  $n_{\text{gal}}^{\text{predicted}}$ , yielding

$$\rho_{pq} = \frac{n_{pq}}{n_{\text{gal}}^{\text{observed}}} \frac{n_{\text{gal}}^{\text{pred}}}{dI/d\rho_{pq}}. \quad (32)$$

It appears that the iterative process is not required in this simplified case. The normalisation of  $\rho_{pq}$  must be determined by multiplying by  $n_{\text{gal}}^{\text{observed}}/n_{\text{gal}}^{\text{pred}}$ , yielding

$$\rho_{pq} = \frac{n_{pq}}{dI/d\rho_{pq}} \quad (33)$$

The final connection is Equation 22 in the limit when  $\Delta M$  is small, such that  $\Omega(m)$  can be assumed to be constant across  $\Delta M$ . As a survey has magnitude limits this can only

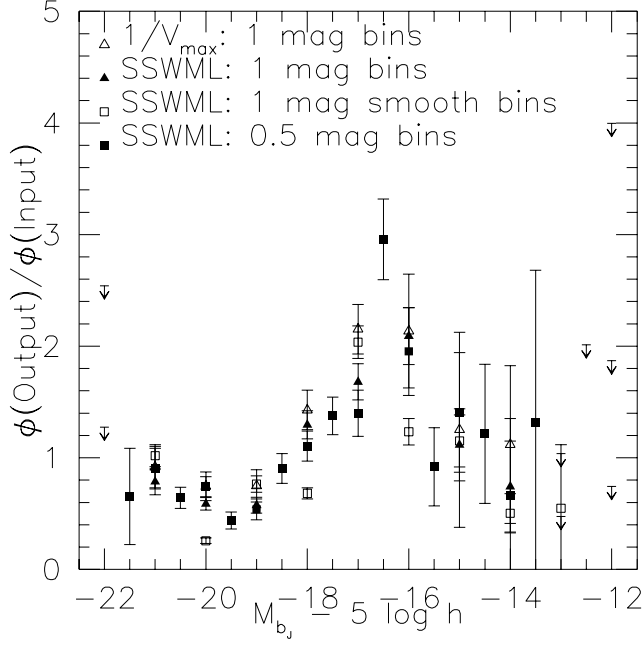


**Figure 9.** Clustered test catalogue of 1800 galaxies. The luminosity function of the clustered test catalogue was determined using a variety of methods (see text).

be an approximation. In this way, the inner integral may be approximated by a product:

$$\begin{aligned} \frac{dI}{d\rho_{pq}} &\approx \int_{z_p - \Delta z/2}^{z_p + \Delta z/2} \Omega(m(z, M_q)) \Delta M \frac{dV}{dz} dz \\ &\approx V_{pq, \text{max}} \Delta M. \end{aligned} \quad (34)$$

Substituting Equation 34 into Equation 33 yields the familiar  $1/V_{\text{max}}$  equation,

$$\rho(z_p, M_q) = \rho_{pq} \approx \frac{n_{pq}}{V_{pq, \text{max}} \Delta M} \quad (35)$$

and we have come full circle — in the limit of small binwidth the SSWML and  $1/V_{\text{max}}$  methods are identical.

Finally, we compare the results of the  $1/V_{\text{max}}$  and SSWML methods when applied to our combined redshift catalogue. Figure 11 compares the redshift evolution of the luminosity function obtained with the  $1/V_{\text{max}}$  method (equivalent to Figure 10 of Paper I, though with broader bins) and that determined using the SSWML method—the agreement is extremely good, as implied by the above discussion. In the rest of this paper we therefore show only the LFs estimated using the SSWML method, although we have checked and found agreement with the  $1/V_{\text{max}}$  method in every case.

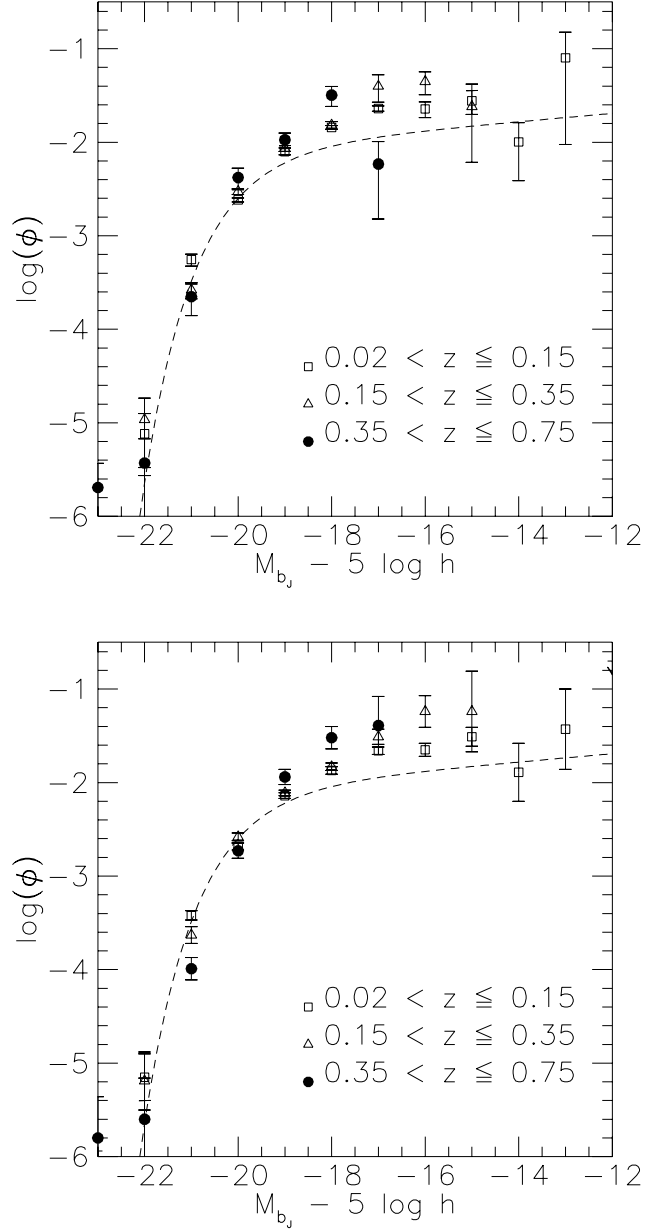


**Figure 11.** Evolution of the luminosity function estimated by the  $1/V_{\text{max}}$  method (top) and the SSWML method (bottom). The luminosity function at several redshifts is depicted by the symbols in the legend with  $1\sigma$  errorbars. The long-dashed curve is the best-fit Schechter function determined by Loveday et al. (1992) without correction for Malmquist bias. All the luminosity function figures that follow have a similar format.

## 5 THE EVOLUTION OF THE LUMINOSITY FUNCTION BY SPECTRAL TYPE

In Paper I (and Figure 11) we demonstrated evolution in the shape of the overall LF since  $z \sim 0.75$ . We present these results again here using both the traditional  $1/V_{\max}$  technique and the clustering-insensitive SSWML method. A comparison of these figures demonstrates that, as we argued in Paper I, the Autofib survey is not grossly affected by clustering. However, the SSWML technique yields a slightly different and a considerably more robust estimate of the galaxy luminosity function.

We also showed in Paper I how the steepening of the faint end slope with look-back time is caused primarily by the population of galaxies with strong [OII] emission, which effectively trace the star-forming component of the field galaxy population. The techniques described in this paper allow us to directly examine the evolution of the galaxy LF as a function of spectral type.

### 5.1 Misclassification and $K$ -correction Error

The analysis in §2.2 shows that the cross-correlation technique may misclassify approximately one-fifth of the spectra in the survey by one spectral class. Therefore before proceeding we must check that such misclassification does not seriously affect our results. To address this, 20% of the galaxies were randomly reclassified by one class blueward or redward, the sampling volumes and absolute magnitudes re-calculated, and the luminosity functions re-determined. Figure 12 presents the results of this test. These luminosity functions agree with those presented in Figure 11 to within the estimated errors, showing that the luminosity functions derived are not sensitive to the level of misclassification present in our sample.

To test the sensitivity to the  $k$ -corrections themselves, we calculate the evolving luminosity function without converting the observed magnitudes to the rest-frames of the galaxies. The evolving observer's frame luminosity function is calculated using the SSWML method (Figure 13). Here, the  $k$ -corrections determined for the surveyed galaxies play no role in the derivation of the luminosity functions. For comparison, we calculate how the observed local distribution of galaxies would appear at higher redshifts if they are observed in the  $B$ -band and binned by their observed  $B$ -band magnitude, i.e. the 'no-evolution' prediction. To perform this comparison we assume a specific local mix of galaxies with varying  $k$ -corrections. As the galaxies suffer larger and larger  $k$ -corrections, the bright-end cutoff luminosity becomes markedly fainter with redshift in both the observations and the model. However, the model predicts fewer faint galaxies than are observed. This effect is analogous to the increase in the faint-end slope in the rest-frame luminosity functions. The number of faint galaxies must therefore increase with look-back time, independent of possible errors in the  $k$ -corrections that we have derived.

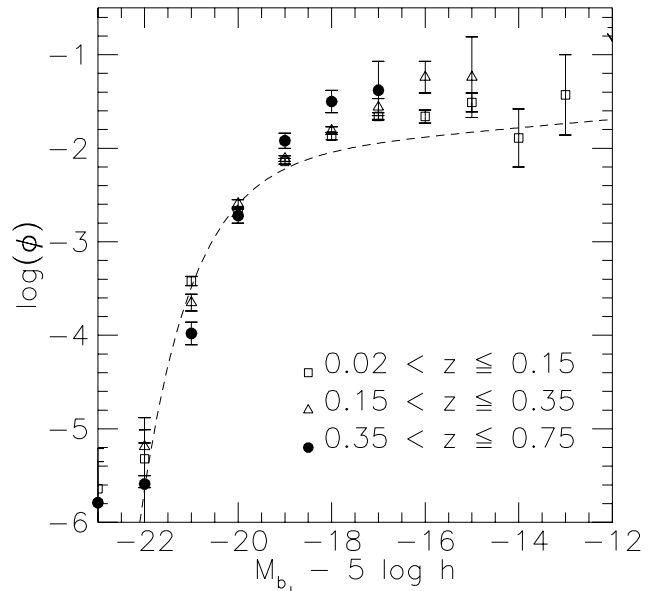


**Figure 12.** Evolution of the luminosity function with 20% random re-classifications by one spectral class.

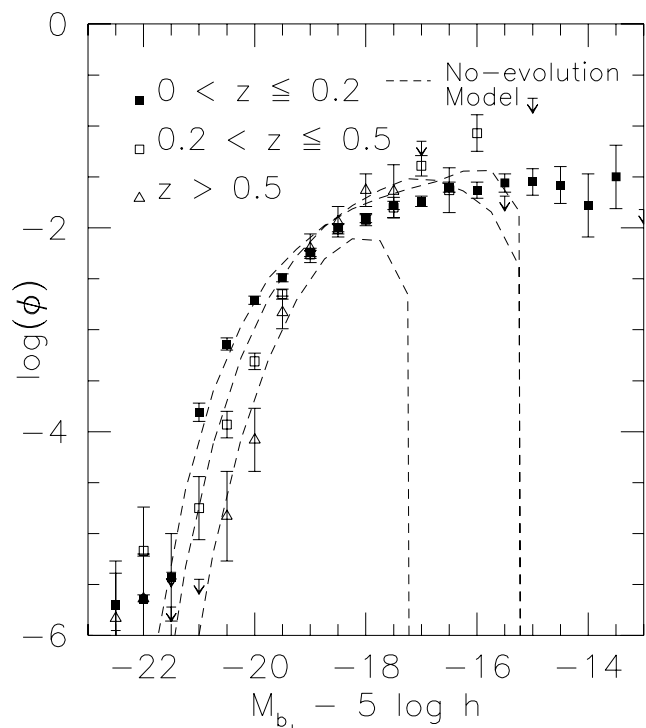


**Figure 13.** Evolution of the luminosity functions in the observer's frame.

## 5.2 Characterising the Evolution

For convenience, we divide the sample into three broad spectral types: E/S0s, early spirals (Sab/Sbc) and late spirals (Scd/Sdm/starburst) in accordance with the discussion in §2. For each of these subsamples we compare the co-added spectra at low and high redshift. The spectra were coadded in the rest-frame with normalisations which are allowed to vary in order to minimise the mean dispersion between the various spectra. Since each spectrum covers a slightly different wavelength range, this is not exactly equivalent to normalising according to the total flux in each spectrum, but the difference only marginally affects the coadded spectra in the range of interest. Because of uncertainties in fluxing these data drawn from such diverse sources, we have made no attempt to flux-calibrate these data. Rather, they are intended to illustrate possible evolution of the *mean spectral features* of the galaxies.

We also determine the LF as a function of redshift for each spectral type by the SSWML method, using a coarser sampling than for the combined sample due to the smaller numbers within each spectral class. As a different approach to characterising the LF evolution of each class, we fit a model for the evolution of the Schechter parameters with redshift using the generalised STY (SSTY) method derived in Equation 9. This is done by maximising the likelihood of observing each subsample assuming the LF evolution takes the following form:

$$\begin{aligned}\phi^*(z) &= \phi_0^*(1+z)^{\gamma_\phi} \\ L^*(z) &= L_0^*(1+z)^{\gamma_L} \\ \alpha(z) &= \alpha_0 + \gamma_\alpha z.\end{aligned}\quad (36)$$

In the above, both the normalisation and characteristic luminosity evolve as a power of cosmic time ( $\phi^* \propto t^{-3\gamma_\phi/2}$  and  $L^* \propto t^{-3\gamma_L/2}$ ), while the faint-end slope evolves linearly with redshift. As with a non-evolving Schechter function, the parameters are highly correlated. The density of galaxies of a given class is given by:

$$\phi(L, z) = \phi_0^*(1+z)^{\gamma_\phi - \gamma_L(\alpha_0 + \gamma_\alpha z)} \left( \frac{L}{L_0^*} \right)^{\alpha_0 + \gamma_\alpha z} \times \exp \left( \frac{-L}{L_0^*(1+z)^{\gamma_L}} \right). \quad (37)$$

For example, if the faint-end slope does not change with redshift ( $\gamma_\alpha=0$ ), then  $\phi_0^*$  and the product  $\alpha_0 L_0^*$  jointly determine the density of faint galaxies as a function of redshift. The correlation of the six parameters makes the errors difficult to interpret. However, although the trends in individual parameters are uncertain, those which determine the overall LF shape are much better determined (at least within the evolutionary formalism adopted). Although the best-fit parameters maximise the likelihood of observing the survey, several sets of these parameters will produce nearly identical trends within the absolute magnitude and redshift range probed.

Furthermore, it is essential to note that the given SSTY model is restricted to monotonic evolution of the parameters with redshift. It will find the trend that the bulk of the galaxies of a given spectral type follow. Since the catalogue is numerically dominated by galaxies at moderate redshift, the SSTY model is most strongly sensitive to the recent evolution of the population.

## 5.3 Early-Type Galaxies

Galaxies with early-type (E/S0-like) spectral classifications represent 20% of the combined survey (331/1603 classified galaxies) and contribute approximately one-tenth of the volume density of intrinsically faint galaxies and one-half of the galaxies with  $L \sim L^*$ .

Figure 14 compares the mean spectra of the E/S0 galaxies with  $0 < z \leq 0.2$  with those  $0.2 < z \leq 0.5$ . At first sight the two spectra appear very similar to each other and also to the E/S0 spectra given in the Kennicutt atlas (Kennicutt 1992a). The most striking differences concern the 4000 Å break and [O II] emission which *both* appear to strengthen with redshift. The former effect is surprising unless there is a selection bias in favour of detecting galaxies with strong features and so cannot be considered a reliable result given the absence of a flux calibration. The presence of the [OII] line in the coadded spectra is more interesting, although it could readily arise from the presence of a few later-type systems with red spectra, as evidenced in the discussion of the precision of our classification system in §2.5.

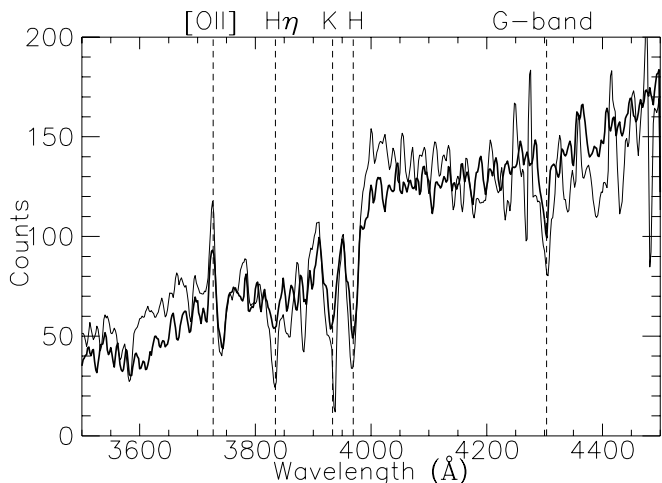
The important point here is the absence of evidence for recent star formation in this predominantly spectrally-inactive class (e.g. a prominent  $H\delta$  line, Zabludoff et al. 1996). This indicates that the bulk of the redder sources in our survey have not recently undergone any star formation on timescales of 1-2 Gyr and thus are passively evolving old systems over the redshift ranges probed.

Figure 15 shows the evolution of the associated LF determined using the SSWML method in three redshift ranges, together with the LFs resulting from SSTY fits for the parameters of the model described above. Neither method finds any convincing evolution of the E/S0 LF out to  $z=0.35$ , while the small sample size at higher redshifts produces large uncertainties and the two methods suggest some evolution, but in opposite senses. The overall conclusion, from both the co-added spectra and the LF analysis, is that there has been little significant change in the properties of the early-type field galaxy population to at least  $z \sim 0.5$ .

## 5.4 Early-Type Spiral Galaxies

Early-type spirals (Sab/Sbc) comprise 40% of the spectrally-classified galaxies (643/1603) and contribute about one-half of the local density of galaxies for luminosities probed by the combined survey. Our analysis proceeds as for the early-type galaxies. Figure 16 compares the coadded spectrum for the





**Figure 14.** Coadded spectra for early-type galaxies. All the galaxies with E/S0 spectral classifications have been coadded in two groups. The bold curve is the coaddition of all early-types with redshifts  $z < 0.2$ . The light curve is for those with  $0.2 < z < 0.5$ . Both spectra have been smoothed on a scale of  $10\text{\AA}$ .

early spirals with  $z < 0.2$  and  $0.2 < z < 0.5$ . An effect similar to that found in the early-types is also evident here, with the absorption lines in the high-redshift spectrum appearing somewhat stronger than in the low-redshift spectrum. The difference between the blue continuum slopes of the two spectra is also in the same direction as in Figure 14 and presumably results from the rapid decrease in the spectrograph response blueward of  $3600\text{\AA}$  which preferentially affects the spectra of the low-redshift galaxies. Again, the principle result is the remarkable similarity of the diagnostic spectral features over this redshift range. We find no significant change in the relative contributions of the Balmer absorption lines or the [OII]  $3727\text{\AA}$  emission line between the low- and high-redshift spectra (the median EWs of [OII] are similar).

However, as Figure 17 shows, there is some modest evolution of the early spirals' LF with redshift. Although there is little or no change in the number of objects with  $L \geq L^*$ , the faint end of the LF steepens as we go to higher redshift. The absence of post-starburst features in the high redshift coadded spectrum indicates the bulk of the population is undergoing constant or smoothly-declining star formation on timescales of a few Gyr.

### 5.5 Late-Type Spiral Galaxies

As shown in Paper I, late-type galaxies appear to be the principal source of evolution in the shape of the overall galaxy LF. In Paper I, the selection method that produced this conclusion was based only on the EW of the [O II] emission line. In fact this selection correlates reasonably closely

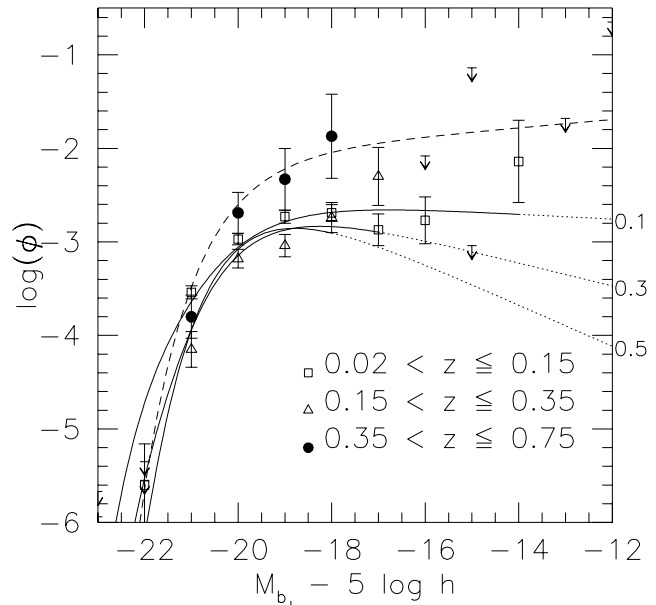


**Figure 15.** The SSWML luminosity functions of E/S0 galaxies in three redshift ranges are shown by the points. The results of the SSTY LF fits for  $z=0.1$ ,  $0.3$  and  $0.5$  are superimposed. The best-fitting monotonically evolving model (found by the SSTY method) underpredicts the number of elliptical galaxies at high redshift relative to the less constrained SSWML results. The Lovejoy et al. (1992) LF (dashed curve) is shown for reference. In this and the subsequent LF figures, we have extrapolated the SSTY LF fits faintward of the observed data to illustrate the trends more clearly. Extrapolations are defined via a dotted line.

with the late-type spiral class discussed here and thus we can anticipate similar results.

Importantly, the coadded spectra for galaxies of this class (Figure 18) shows a marked change in the nature of the star formation present. As originally discussed by Broadhurst, Ellis & Shanks (1988), the higher redshift spectrum shows much deeper  $H\delta$  absorption and a possible reversal of the Ca II line ratio suggesting the presence of a stronger  $H\epsilon$ ; these lines are signatures of more recent ( $\approx 1$  Gyr) star formation. Coupled with this is a strong increase in the strength of the [O II] emission. These diagnostics suggest such galaxies are being seen at an atypical stage in their star formation history.

Figure 19 reveals the [O II] evolution more clearly: at fixed luminosity there is an increase in the median [OII] EW with redshift. This effect is superimposed upon the well-known tendency for fainter objects to have stronger emission. Analysing objects in a narrow range of spectral type minimises the bias arising from the fact that fainter samples become more dominated by such galaxies because of the  $k$ -correction (Koo & Kron 1992). Taking [OII] EW as an

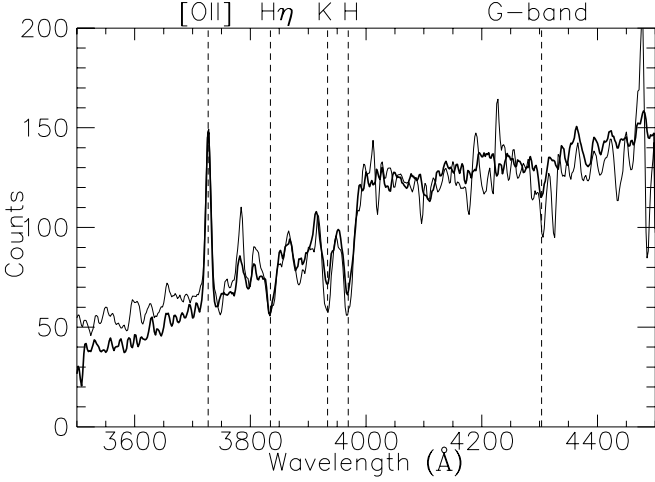


**Figure 16.** Coadded spectra for early-type spiral galaxies. The bold curve is the coaddition of all early spirals with redshifts  $z < 0.2$ , while the light curve is those with  $0.2 < z < 0.5$ . Both spectra have been smoothed on a scale of  $10\text{\AA}$ .

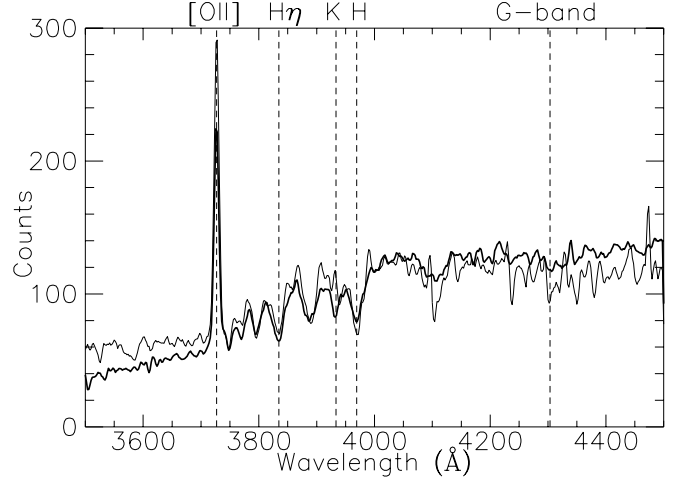


**Figure 18.** Coadded spectra for late-type spiral galaxies. The bold curve is the coaddition of all late spirals with redshifts  $z < 0.2$ , while the light curve is those with  $0.2 < z < 0.5$ . Both spectra have been smoothed on a scale of  $10\text{\AA}$ .

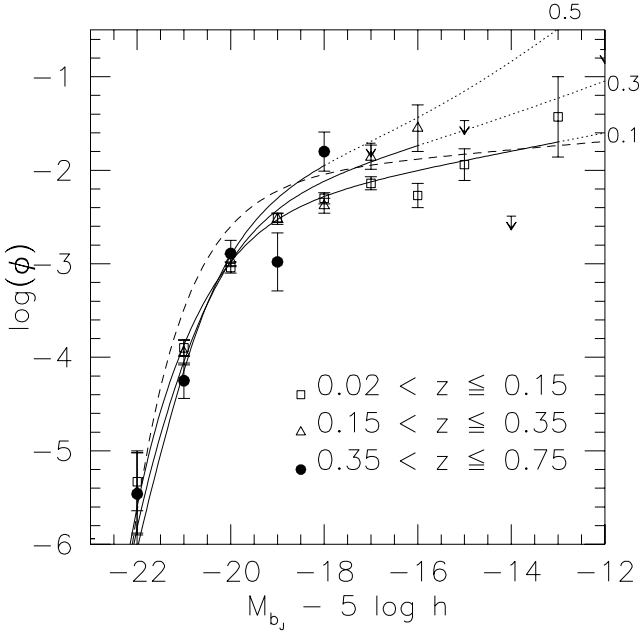


**Figure 17.** SSWML luminosity function of early spiral galaxies. The results of the generalised STY fitting for the early-type spirals are superimposed for  $z=0.1$ ,  $0.3$  and  $0.5$ .

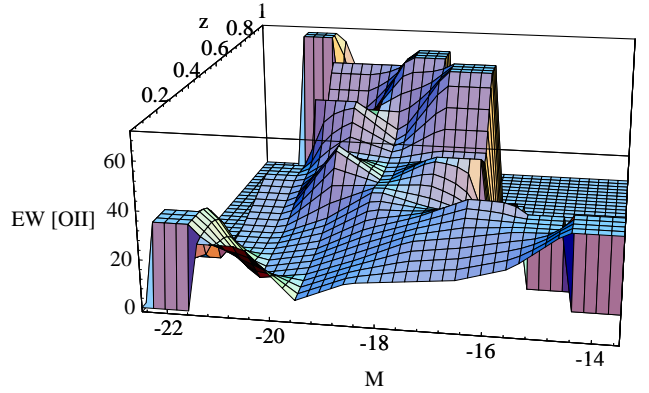


**Figure 19.** Evolution of the median [OII] EW for late-type spirals. In regions of the  $M_B - z$  where no galaxies were observed, a median EW of  $0\text{\AA}$  is plotted.

indicator of star-formation rate, we can therefore conclude that in late-type spirals the star-formation rate is higher in lower luminosity objects at fixed redshift and higher in higher redshift objects at fixed luminosity. Alternatively, a given star-formation rate is found at higher redshift in higher luminosity objects. The spectra indicate the nature of star formation changes also, becoming more ‘burst-like’ in the distant samples.

The evolution of the late-type spirals dominates the more modest changes seen in the LFs of the other types. Their density and faint-end slope both increase with redshift, while the cutoff luminosity remains fixed. Consequently they contribute an increasing fraction at all luminosities, progressively dominating the population at brighter

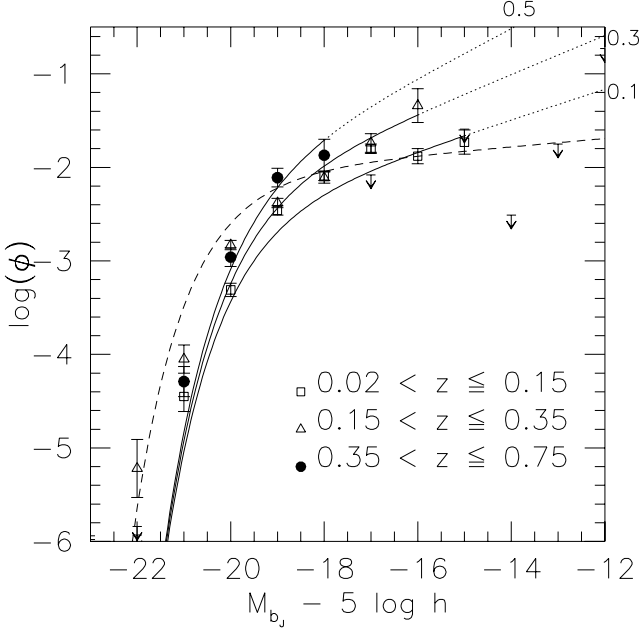


**Figure 20.** SSWML luminosity function of late spiral galaxies. The results of the generalised STY fitting for the late-type spirals are superimposed for  $z=0.1$ ,  $0.3$  and  $0.5$ .

limits and by  $z \sim 0.5$  becoming the most common galaxy type at all luminosities below  $L^*$ .

### 5.6 Summary and a Check

The evolution of the various galaxy types is summarised in pictorial form in Figure 21. This characterisation goes further than in the preceding sections and provides SSTY characterisations of the LF evolution for each of *six* spectral classes. With this level of subdivision the LFs are individually highly uncertain even within the framework of the assumed evolutionary form (especially for the early-type class which is poorly represented at high redshift). Nonetheless the figure illustrates that the earlier spectral types only weakly evolve whereas the rate of change is greatest for the later types. It is also clear that the evolution takes the form of a steepening of the faint end of the LF with  $L^*$  galaxies only being significantly affected at  $z \sim 0.5$ . The parameters of the SSTY fits are provided in Table 2, although, in light of the above caveats, should clearly be used and interpreted with caution.

As a final check, the SSTY LF fits for each spectral type are combined to give the evolution of the overall luminosity function. This is compared to the SSWML LFs for the whole sample in Figure 22 and the consistency check demonstrates that for the large combined sample the two approaches yield consistent results. We conclude that the

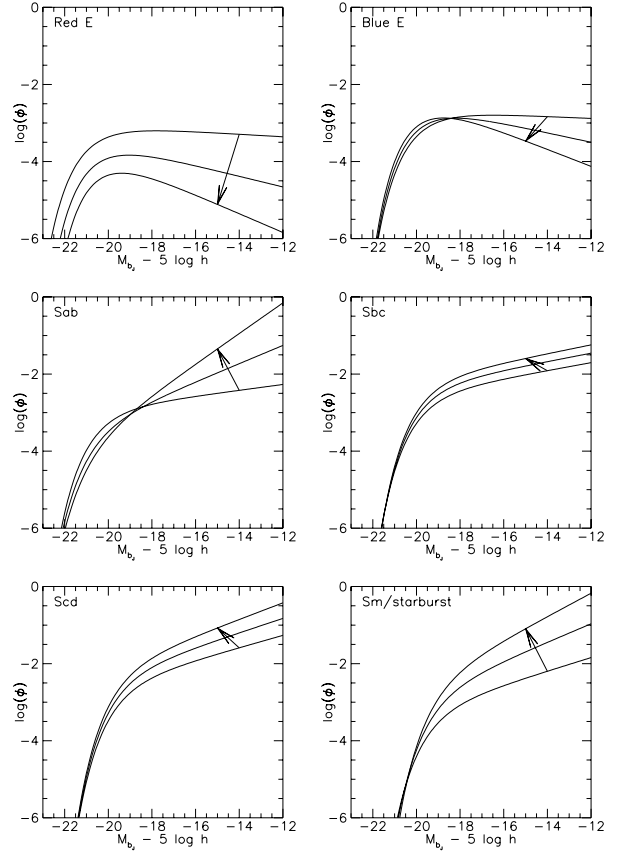


**Figure 21.** The evolution of the luminosity function by spectral type. The curves trace schematically the best-fitting, monotonically evolving luminosity functions determined by the SSTY method at  $z=0.1$ ,  $0.3$  and  $0.5$ . Arrows indicate increasing redshift.

evolutionary framework assumed in the SSTY fits is sufficiently general to adequately match the observations.

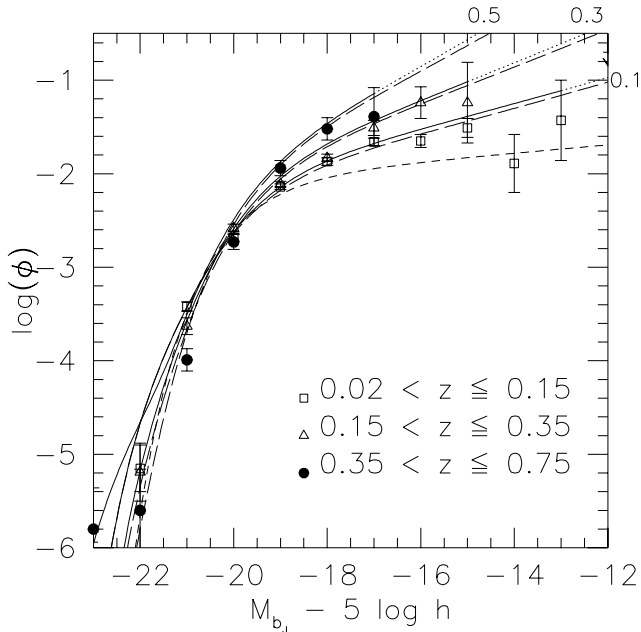
## 6 DISCUSSION

The evolution of the LF by spectral type described in the previous section considerably extends the analyses of previous studies, which have either used [OII] EW (Paper I) or red/blue colour (Lilly et al. 1995) to make a simple distinction between the star-forming and quiescent galaxy populations. Comparison of those studies with the more detailed results presented here, however, shows broad agreement. The analyses based here will pave the way for more comprehensive analyses that will become possible in more extensive homogeneous faint spectral surveys.

In comparing the LF evolution of the red and blue galaxies in their  $I < 22$  redshift survey, Lilly et al. (1995) found that there was very little change in the luminosity or number density of the red galaxies over the whole red-

**Table 2.** The evolution of the LF parameters.

Type	$\phi_0^*$ (Mpc $^{-3}$ )	$\gamma_\phi$	$M_0^*$	$\gamma_L$	$\alpha_0$	$\gamma_\alpha$
Red E	$1.62 \times 10^{-3}$	-6.15	-20.7	-1.77	-1.05	1.31
Blue E	$1.87 \times 10^{-3}$	1.56	-19.57	-0.35	-1.06	1.23
Sab	$2.19 \times 10^{-3}$	-4.44	-20.0	0.92	-0.99	-2.01
Sbc	$2.80 \times 10^{-3}$	2.89	-19.4	-0.37	-1.25	-0.07
Scd	$3.01 \times 10^{-3}$	3.48	-19.2	-0.18	-1.37	-0.34
Sdm/Starburst	$0.50 \times 10^{-3}$	6.61	-19.0	-0.97	-1.36	-0.79

**Figure 22.** Comparison of the SSTY and SSWML luminosity functions. The sum of the SSTY LFs for the six classifications and the unclassified galaxies (the solid curves) is compared with the LF for all the galaxies in the survey as determined by the SSWML method. The Loveday et al. (1992) LF is shown as the short-dashed curve. Just below the solid curves are long-dashed curves, which show the evolution of the luminosity function with unclassified galaxies excluded from the analysis. The SSTY results are given for  $z=0.1, 0.3$  and  $0.5$ .

shift range  $0 < z < 1$ , a point which we can confirm both in terms of the derived LF and the mean spectral characteristics. Amongst the blue galaxies Lilly et al. (1995) found substantial evolution at  $z > 0.5$ , so that by  $0.5 < z < 0.75$  the blue LF had brightened by about 1 mag. They were non-committal about the evolution of the blue LF at lower redshifts, due to the small number of objects at  $z < 0.2$  (35) with which to compare their  $0.2 < z < 0.5$  LF. Nonetheless, their Schechter function parameters indicated that the blue galaxies with  $z < 0.5$  (which are mostly at the high end of our redshift range) have a LF with a faint-end slope  $\alpha$  between  $-1.3$  and  $-1.6$ . This is as steep or steeper than the value

we obtain for low-redshift mid- to late-type spirals in our SSTY parametric analysis (see Table 3), but quite consistent with the values we find for these types at  $z \lesssim 0.5$ . With a much larger sample at lower redshifts, our results not only show that significant evolution is occurring at  $z < 0.5$ , but also demonstrate the marked type-dependence, with late-type spirals evolving more strongly than mid-type spirals.

Many authors have previously postulated that late-type galaxies are the prime movers in the evolution of the luminosity function as appears to be manifest in the number-magnitude relation. Their blue colours imply that they are least affected by  $k$ -corrections and thus can be observed to the largest distances for a given absolute magnitude. Broadhurst, Ellis & Shanks (1988) found that a luminosity function with a constant cutoff luminosity and a faint-end slope which increases with redshift is consistent with both the slope of the observed blue number counts and the redshift distribution. Lacey & Silk (1991) and Treyer & Silk (1994) both supported this finding, and conjectured that these changes are driven by blue, late-type galaxies which have disappeared since a redshift of  $z \sim 0.2$ . Lacey & Silk (1991) propose several options for their disappearance.

The excess galaxies could have produced more high-mass stars proportionally than modern galaxies. This bias toward high-mass stars would make them brighter while stars were forming, but the galaxies would quickly fade after the high-mass stars became supernova, leaving few stars to be observed today. An alternative explanation is that these galaxies have merged into the galaxies that we observe today. White (1990) and Efstathiou (1990) argue that such an evolutionary history is a natural consequence of the turnaround of larger and larger mass scale with time in a hierarchical universe. However, large amounts of merging would leave traces in today's galaxies which are not observed (Toth & Ostriker 1992). Furthermore, these excess galaxies are unlikely to be the progenitors of today's galaxies as they are more weakly clustered and more dense than galaxies today (Babul & Rees 1991). However, there is no convincing evidence in either our early-type spectra or LFs for a significant build up of more massive early types (c.f. Dalcanton(1993)) as would be the case in the merger hypotheses.

Babul & Rees (1991) propose a further explanation (elucidated also in Efstathiou 1992). Although small mass haloes ( $\sim 10^9 M_\odot$ ) collapse and virialise before the nascent haloes of  $L^*$  galaxies, the UV flux produced by quasars may keep the gas in small haloes ionised until  $z \sim 1$ . Only then can these

small galaxies begin to form stars. Such stars would form quickly as in a starburst galaxy. During the starburst these galaxies would appear irregular and their spectra would be similar to those of present-day late-type spirals (i.e. dominated by short-term stellar activity). Supernovae would blow out the gas, halting the star formation rate, and the galaxy would begin to fade (more quickly in the  $B$ -band than in the  $K$ -band). Babul & Rees (1991) also proposed that in low-pressure environments the gas may escape the galaxy entirely, while in intermediate and high-pressure regions, some gas might return to the galaxy, possibly fuelling further events. The few galaxies that could still be observed today would be in the high-pressure regions clustered near more luminous galaxies. Gigayears of phase mixing could transform these irregular starburst galaxies into today's population of dwarf elliptical galaxies. However, the vast majority of these remnant irregulars would fade below detection limits. Although the clear proof of this picture would be the identification of an abundant population of local remnants, presumably via deep infrared imaging, the short-term nature of star formation in the coadded spectra of the dominant evolutionary component provides some support for this picture. With the larger databases anticipated in the forthcoming deep surveys, it will hopefully become possible to tie the timescales observed in the redshift evolution to those indicated by the detailed spectral features in the coadded spectra.

## 7 CONCLUSIONS

This paper investigates the evolution of the galaxy luminosity function for galaxies of different spectral types. The analysis is based on the Autofib redshift survey described in Ellis et al. (1996) and uses new techniques developed for spectral classification and for recovering the luminosity function in the presence of both evolution and clustering.

We classify the redshift survey galaxies into six spectral types using a cross-correlation method that simulations show correctly assigns the type for 80% of the sample and is out by at most one type more than 90% of the time. These types compare well with those derived from the galaxies' colours and, where available, with Hubble Space Telescope morphologies.

We describe an extension of the step-wise maximum likelihood method for estimating luminosity functions, rigorously testing the method and comparing its performance to the standard  $1/V_{\max}$  method. Significant advantages to the new SSWML method are found in reducing the sensitivity of the results to clustering. We also describe an extension to the Sandage, Tammann & Yahil (1979) method that enables us to recover the best fit to a parametric model for the luminosity function including its evolutionary behaviour.

Applying these methods to the Autofib redshift survey we obtain the following main results:

1. There is no significant evolution in the mean spec-

trum or luminosity function of early-type galaxies out to at least  $z \sim 0.5$ . This significantly constrains the continued production of such galaxies (e.g. via mergers of star-forming galaxies over the last few Gyr).

2. Early-type spiral galaxies show relatively modest evolution which is well-characterised by a simple steepening of the faint end of their luminosity function with redshift. Early spirals show little evidence for evolution of either  $L^*$  or  $\phi^*$  over this redshift range. Their spectra at all redshifts sampled are consistent with smooth changes in the overall star formation history.

3. Out to  $z \sim 0.5$ , the overall evolution of the galaxy population is dominated by the evolution of late-type spirals. Their luminosity function not only steepens and brightens (evolution of both  $\alpha$  and  $L^*$ ) but there are also signs of significant density evolution (a rapid increase in  $\phi^*$ ). There appears to be a qualitative change in the spectra of late type spirals with redshift. In addition to a rise in the median [OII] equivalent width, a greater proportion of high redshift sources show Balmer line ratios indicative of short-term star formation. Coupled to the increase in star-formation rate at lower luminosities at fixed redshift, this implies that a given star-formation rate is found at higher redshift in higher luminosity objects.

## ACKNOWLEDGEMENTS

We acknowledge useful discussions with Len Cowie, Simon Lilly, Olivier LeFevre, Donald Lynden-Bell and David Koo. We thank Jarle Brinchmann and Karl Glazebrook for assistance with analyses of the HST images. JSH thanks the Marshall Aid Commission. MMC acknowledges the assistance of the Australian Academy of Science/Royal Society exchange program. RSE and KGB acknowledge financial support from PPARC.

## REFERENCES

- Abraham R.G., Tanvir N.R., Santiago B.X., Ellis R.S., Glazebrook K., van den Bergh S., MNRAS, 279, L47.
- Avni Y., Bahcall J.N., 1980, ApJ, 235, 694
- Babul A., Rees M.J., 1991, MNRAS, 255, 346
- Bender R., Burstein D., Faber S.M., 1993, ApJ, 411, 153
- Binggeli B., Sandage A., Tammann G.A., 1988, ARA&A, 26, 509
- Broadhurst T.J., Ellis R.S., Shanks T., 1988, MNRAS, 235, 827
- Cholowiecki J., 1986, MNRAS, 223, 1
- Colless M.M., Ellis R.S., Taylor K., Hook R.N., 1990, MNRAS, 244, 408
- Colless M.M., Ellis R.S., Broadhurst T.J., Taylor K., Peterson B.A., 1993, MNRAS, 261, 19
- Cowie L.L., Songaila A., Hu E.M., 1991, Nature, 354, 460
- Dalcanton J.J., 1993, ApJ, 415, L87
- deVaucouleurs, G., 1977, in Tinsley B.M. & Larson R.B., ed., The Evolution of Galaxies and Stellar Populations, Yale University Observatory, New Haven, p.43
- Eales S., 1993, ApJ, 404, 51

- Efstathiou, G., 1990, in Wielen R., ed., Dynamics and Interactions of Galaxies, Springer, Berlin, p.2
- Efstathiou G., 1992, MNRAS, 256, 43P
- Efstathiou G., Ellis R.S., Peterson B.A., 1988, MNRAS, 232, 431
- Ellis R.S., Colless M.M., Broadhurst T.J., Heyl J.S., Glazebrook K., 1996, MNRAS, 280, 235, (Paper I)
- Felten J.E., 1976, ApJ, 207, 700
- Glazebrook K., Ellis R.S., Colless M.M., Broadhurst T.J., Allington-Smith J.R., Tanvir N.R., 1995a, MNRAS, 273, 157
- Glazebrook K., Ellis R. S., Santiago B. X., Griffiths R. E. 1995b, MNRAS, 275, L19
- Heyl J.S., 1994, M.Sc. Thesis, University of Cambridge
- Kennicutt R., 1992a, ApJS, 79, 255
- Kennicutt R., 1992b, ApJ, 388, 410
- King C.R., Ellis R.S., 1985, ApJ, 288, 456
- Kinney, A. L., Bohlin, R. C., Calzetti, D., Panagia, N. & Wyse, Rosemary F. G 1993, ApJS, 86, 5
- Koo D.C., Kron R.G., 1992, ARA&A, 30, 613
- Lacey C.G., Silk J., 1991, ApJ, 381, 14
- Lilly S.J., Tresse L., Hammer F., Crampton D., Le Fevre O., 1995, ApJ, 455, 108
- Lin H., Kirshner R.P., Sheckman S.A., Landy S.D., Oemler A., Tucker D.L., Schechter P.L., 1996, ApJ, in press
- Lonsdale C.J., Chokshi A., 1993, AJ, 105, 1333
- Loveday J., Peterson B.A., Efstathiou G., Maddox S.J., 1992, ApJ, 390, 338
- Lynden-Bell D., 1971, MNRAS, 155, 95
- Marshall H.L., Avni Y., Tananbaum N., Zamorani G., 1983, ApJ, 269, 35
- Marzke R.O., Geller M.J., Huchra J.P., Corwin H.G., 1994, AJ, 108, 437
- Pence W., 1976, ApJ, 203, 39
- Peterson B.A., Ellis R.S., Bean A.J., Efstathiou G.P., Shanks T., Fong R., Zou Z-L., 1985, MNRAS, 221, 233.
- Sandage A., Tammann G.A., Yahil A., 1979, ApJ, 232, 352
- Saunders W., Rowan-Robinson M., Lawrence A., Efstathiou G., Kaiser N., 1990, MNRAS, 242, 318
- Schmidt M., 1968, ApJ, 151, 393
- Taylor K., 1995, BAAS, 186, #44.06
- Toth G., Ostriker J.P., 1992, ApJ, 389, 5
- Treyer M.A., Silk J., 1994, ApJ, 436, L143
- White S.D.M., 1990, in Wielen R., ed., Dynamics and Interactions of Galaxies, Springer, Berlin, p.380
- Zabludoff A.I. et al. 1996, "The Environment of E+A Galaxies," LANL Preprint: astro-ph/9512058, ApJ, submitted.
- Zaritsky, D., Zabludoff, A.I., Willick, J.A. 1995, AJ, 110, 1602.